AppliedMath

MDPI

*Article*

# A Game-Theoretic Framework for PI/PID Controller Selection in a Coupled Two-Tank Hydraulic System

**Nacim Nait Mohand [1,*] and Hocine Lehouche [2]**

[1] Research Unit LaMOS (Modeling and Optimization of Systems), Faculty of Technology, University of Bejaia, Bejaia 06000, Algeria
[2] Laboratory of Industrial and Information Technology (LTII), Faculty of Technology, University of Bejaia, Bejaia 06000, Algeria; hocine.lehouche@univ-bejaia.dz
* Correspondence: nacim.naitmohand@univ-bejaia.dz; Tel.: +213-671-839-161

**Abstract**

This paper addresses loop-wise PI/PID controller structure selection in a coupled two-tank hydraulic system. Existing studies generally prescribe controller architectures or compare predefined configurations after synthesis, leaving this problem insufficiently explored when each choice depends energetically on the neighboring loop. Although exact feedback linearization decouples the auxiliary tracking dynamics, the reconstructed physical pump inputs retain nonlinear hydraulic coupling. Consequently, reducing the control energy of one loop may increase the effort required by the other, creating conflicting local objectives that motivate a non-cooperative game-theoretic formulation. The plant is feedback-linearized, PI and PID controllers are parameterized by pole placement, and their assignment is posed as a finite static game in which each player minimizes pump energy cost. For the nominal symmetric configuration, (PID, PID) is the unique Nash equilibrium, although (PI, PI) yields a lower aggregate control energy cost (291.4134 vs. 291.8184), showing that unilateral optimality does not coincide with collective energy minimization. PID reduces settling time from 5.253 s to 3.422 s (34.9%) but increases maximum overshoot from 13.55% to 20.82% (53.7%). Sensitivity analyses show that tuning, leakage, coupling, and initial conditions can reverse best responses, while a $\pm 10\%$ parametric mismatch analysis preserves convergent tracking with small steady-state errors, although the equilibrium may change.

**Keywords:** coupled two-tank system; feedback linearization; PI/PID control; game theory; Nash equilibrium; controller selection; hydraulic systems; nonlinear systems

## 1. Introduction

Hydraulic level control systems are widely encountered in industrial process engineering, water management, energy systems, and automated production. In these applications, reliable regulation must be achieved despite nonlinear flow characteristics, interactions among interconnected units, modeling uncertainties, and external disturbances. Coupled tank systems constitute a representative benchmark for investigating these challenges and for assessing nonlinear and advanced control strategies [1–3]. Their dynamics arise from mass conservation principles and nonlinear hydraulic relations derived from Bernoulli's principle and Torricelli-type flow laws [4]. In particular, the hydraulic exchange between interconnected tanks depends on the difference between their liquid levels; consequently, the evolution of each level depends not only on its local inflow and outflow rates but also on the state of the neighboring tank.

Check for updates

Received: 7 July 2026
Revised: 2 September 2026
Accepted: 2 September 2026
Published: 8 September 2026

**Copyright:** © 2026 by the authors. Licensee MDPI, Basel, Switzerland. This article is an open access article distributed under the terms and conditions of the Creative Commons Attribution (CC BY) license.

To address the nonlinearities inherent in such dynamical systems, state feedback linearization provides a systematic and well-established framework. When a sufficiently accurate process model is available, this approach can compensate for known nonlinear terms and transform the original dynamics into a simpler auxiliary representation suitable for control synthesis [5]. Once this representation is obtained, classical techniques such as pole placement can be employed to prescribe the desired closed-loop dynamics [6]. These tools provide an effective basis for nonlinear compensation and controller parameterization, but do not by themselves determine which controller structure should be assigned to each control loop.

This distinction becomes particularly important in coupled hydraulic systems, where selection of the controller structure cannot be separated from the physical interactions between subsystems. A controller structure that modifies the trajectory of one tank also modifies the hydraulic exchange through the interconnection, and may consequently alter the physical control effort required by the neighboring actuator. In general, the suitability of a given controller structure for one loop cannot be assessed independently of the structure selected for the other loop. Thus, even when the nonlinear dynamics are transformed into a simpler form for control design, the underlying hydraulic interconnection can preserve the dependence of the physical consequences of one local controller choice on the choice made by the neighboring loop. For this reason, controller structure selection must be regarded as a distinct design problem involving mutually dependent decisions across the interacting control loops.

For coupled tank level regulation, proportional–integral (PI) and proportional–integral–derivative (PID) controllers remain prominent because of their simple implementation, interpretable tuning parameters, and practical effectiveness. Building on this foundation, the literature has progressed along three complementary directions: advanced controller synthesis and tuning; treatment of interactions, uncertainties, and disturbances; and comparative assessment of alternative control architectures.

A first line of research seeks to enhance conventional PI/PID control through fractional-order formulations and optimization-based tuning. Roy and Roy [7] developed a fractional-order PI controller with feedforward compensation for a coupled two-tank MIMO system and experimentally benchmarked it against PI, PID, 2DOF-PI, and 3DOF-PI configurations. Roy et al. [8] investigated a cascaded FOPI–FOPD architecture; under identical phase-margin and gain-crossover-frequency specifications, they reported lower steady-state error and control energy than its integer-order counterpart. Sorcia-Vázquez et al. [9] implemented continuous- and discrete-time FOPID controllers in real time and optimized their parameters using genetic algorithms with an objective function combining tracking error and control effort. These studies show that performance gains can be achieved through advanced parameterization and fractional-order extensions while keeping the controller architectures predefined and tuning or optimizing their parameters.

A second line of research addresses multivariable interactions, uncertainty, disturbance rejection, and robustness in interconnected liquid level systems. Govind and Mahapatra [10] designed decentralized PI/PID controllers for decoupled subsystems from frequency-domain specifications and assessed robustness to input and output multiplicative uncertainties. Meng et al. [11] combined input–output feedback linearization with a nonlinear disturbance observer in a quadruple-tank system to estimate and compensate for unknown disturbances, achieving improved dynamic and steady-state performance over conventional PID and disturbance observer-based sliding-mode control in simulation and experiments. In [12], Govind and Mahapatra extended their earlier framework by combining decouplers, PID tuning based on tree seed optimization, and $\mu$-analysis to improve nominal performance under uncertainty. Ünal et al. [13] addressed uncertain

time-varying input delays through a robust least-fragile PI design. These contributions explicitly account for interactions, uncertainties, and disturbances, yet primarily seek to attenuate or accommodate them within a prescribed control architecture.

A third line of research examines the consequences of selecting among alternative controller architectures. Ayten et al. [14] experimentally compared FF-PI, cascaded nonlinear PI-based, and fractional-order adaptive sliding-mode strategies on a double-tank process, revealing differences in tracking, disturbance rejection, and transient response. Nursoy and Başçi [15] compared classical PI with Type-1 and interval Type-2 fuzzy PI controllers in real time using transient characteristics and integral error indices, whereas Yesil and Sahin [16] evaluated FLC, feedback linearization-based PID, and feedback linearization-based FLC on a physical coupled-tank platform and identified trade-offs among overshoot, settling time, and tracking accuracy. While these comparisons confirm that the controller architecture materially affects closed-loop behavior, alternatives are generally assessed as predefined process-level configurations rather than as structural choices assigned separately to interacting loops.

Taken together, these contributions reveal a clear distinction between improving a controller once its architecture has been specified and deciding which architecture should be assigned to each loop of an interconnected system. Existing studies have substantially advanced controller tuning, interaction mitigation, disturbance rejection, robustness, and comparative performance assessment; however, controller structures are still predominantly treated either as predefined design choices or as alternative configurations to be evaluated after synthesis. This leaves a distinct question insufficiently explored: how should controller structures be selected at the level of the individual loop when the physical consequences of each choice depend on the structure adopted by the neighboring loop? In a coupled hydraulic system, such dependence is particularly relevant because a structural choice that changes the trajectory of one tank can modify the interconnection flow, and consequently the control effort required by the other actuator. In general, the appropriate controller structure for one loop cannot be identified solely from its isolated performance; therefore, the design problem shifts from ranking independently evaluated controller alternatives to determining a combination of local structures for which the consequences are mutually dependent. From this perspective, controller architecture becomes an interdependent decision variable rather than a fixed prerequisite of controller design.

Game theory provides a modeling framework for recasting the interdependence among local decisions as an explicit decision problem in which the players, their strategies, their objectives, and the relevant solution concept are defined according to the physical and informational structure of the interaction. In interconnected hydraulic systems, game-theoretic formulations have been employed to address different forms of coupling, decentralization, uncertainty, and strategic interaction. Hajji et al. [17] formulated distributed nonlinear model predictive control of a nonlinear four-tank system within a cooperative game-theoretic framework where coalition formation is used to coordinate the decisions of dynamically coupled subsystems. Umsonst et al. [18] considered a sensor attack–defense problem numerically evaluated on a four-tank process and modeled the interaction as a simultaneous-move Bayesian game; the Bayesian Nash equilibrium was then used to determine a defense strategy that accounts for uncertainty regarding the attacker's objective. More recently, Misra et al. [19] formulated decentralized control of a water distribution system as a Markov game and sought an approximate correlated equilibrium among local controllers. Collectively, these studies illustrate how the game structure and associated solution concept can be tailored to the nature of the interaction, the information available to the decision-makers, and the organization of their decisions.

Guided by this principle, the present work formulates controller structure selection as an interdependent decision problem for two hydraulically coupled regulation loops. The process consists of two vertical tanks supplied by independent pumps and interconnected through a hydraulic channel, and is subject to external leakage. The nonlinear dynamics of the process are derived from mass conservation and standard hydraulic flow relations, then transformed by exact state-feedback linearization into an auxiliary representation used for control synthesis. PI and PID controllers are parameterized for each loop via pole placement. Each tank is associated with one player, whose strategy set comprises the two candidate controller structures and whose objective is to minimize the energy required by its physical pump input.

The proposed game is non-cooperative because the two regulation loops act through independent pumps and are evaluated according to the energy required by their respective actuators. No supervisory mechanism is introduced to negotiate controller architectures or redistribute control effort between the loops. The formulation is static because the PI or PID architecture is selected at the design stage and retained throughout operation; although the hydraulic states and control signals evolve continuously, the controller structures themselves remain fixed. The structural decisions are modeled as simultaneous because both loops operate over the same control horizon and neither has a physical, organizational, or informational priority that would justify a leader–follower hierarchy. Nash equilibrium is adopted because the selected architecture for each loop should remain preferable in terms of its own actuator energy requirement when the architecture assigned to the neighboring loop is kept fixed. Finally, the analysis focuses on pure-strategy equilibria because the intended engineering outcome is a definite and directly implementable PI or PID architecture for each loop.

The main contributions of this work are summarized as follows:

1. Controller structure selection is formulated at the level of individual loops as a finite game in which each loop selects between PI and PID. Selection is carried out according to the energy required by its physical pump input while accounting for the influence of the neighboring controller structure.
2. The framework distinguishes between the decoupled auxiliary dynamics obtained through exact feedback linearization and the physical pump inputs, for which hydraulic coupling preserves the interdependence of the local energy costs.
3. PI and PID structures are assessed in the time domain through maximum overshoot, settling time, and finite-horizon steady-state error, complementing the energy-based game-theoretic analysis.
4. Sensitivity analyses with respect to controller tuning, leakage, hydraulic coupling, and initial conditions are carried out to evaluate their respective effects on control costs, time-domain performance, best responses, and Nash equilibria, while a robustness analysis under parametric model uncertainties assesses the effect of imperfect nonlinear compensation on tracking performance and strategic controller selection.

The remainder of this paper is organized as follows: Section 2 presents the mathematical model of the coupled two-tank system; Section 3 develops the feedback-linearization procedure and PI/PID controller design; Section 4 formulates the controller structure selection game and characterizes its Nash equilibria; Section 5 presents the numerical results, sensitivity analyses, and robustness assessment under parametric model uncertainties; finally, Section 6 concludes the paper.

## 2. Mathematical Modeling of the Interacting Two-Tank System

This section presents the mathematical model of the interacting two-tank hydraulic system. First, the physical configuration is described, followed by the main modeling

assumptions and hydraulic flow laws, leading to a nonlinear state-space representation of the system. The resulting model is then analyzed in terms of its equilibrium conditions, nonlinear characteristics, and the influence of hydraulic coupling on local stability.

### *2.1. Physical Configuration of the Hydraulic System*

We consider a hydraulic system composed of two interconnected vertical tanks, denoted by $R_1$ and $R_2$. The liquid levels in the two tanks are denoted by $y_1(t)$ and $y_2(t)$, respectively. Each tank is supplied by an independent pump. The inlet flow rates of the pumps are respectively denoted by $u_1(t)$ and $u_2(t)$. These flow rates constitute the control inputs of the system.

For each tank $R_i$, $i \in \{1,2\}$, $u_i(t)$ represents the volumetric flow rate delivered by pump $i$ into the tank; it therefore enters the corresponding mass balance equation as a positive inflow.

Tanks $R_1$ and $R_2$ are connected through an interconnection channel with cross-sectional area $a$, where $a \geq 0$, allowing fluid exchange between the two tanks.
The corresponding signed interconnection flow rate is denoted by $Q_{12}(t)$, with the positive direction defined from $R_1$ to $R_2$. In addition, each tank $R_i$, $i \in \{1,2\}$, is equipped with an external outlet of cross-sectional area $b_i$, where $b_i \geq 0$, through which the liquid can leave the system. The associated external outlet flow rate is denoted by $Q_{i,\text{ext}}(t)$.

The liquid levels $y_1(t)$ and $y_2(t)$ are assumed to be measurable by level sensors. Figure 1 illustrates the physical structure of the considered hydraulic system.

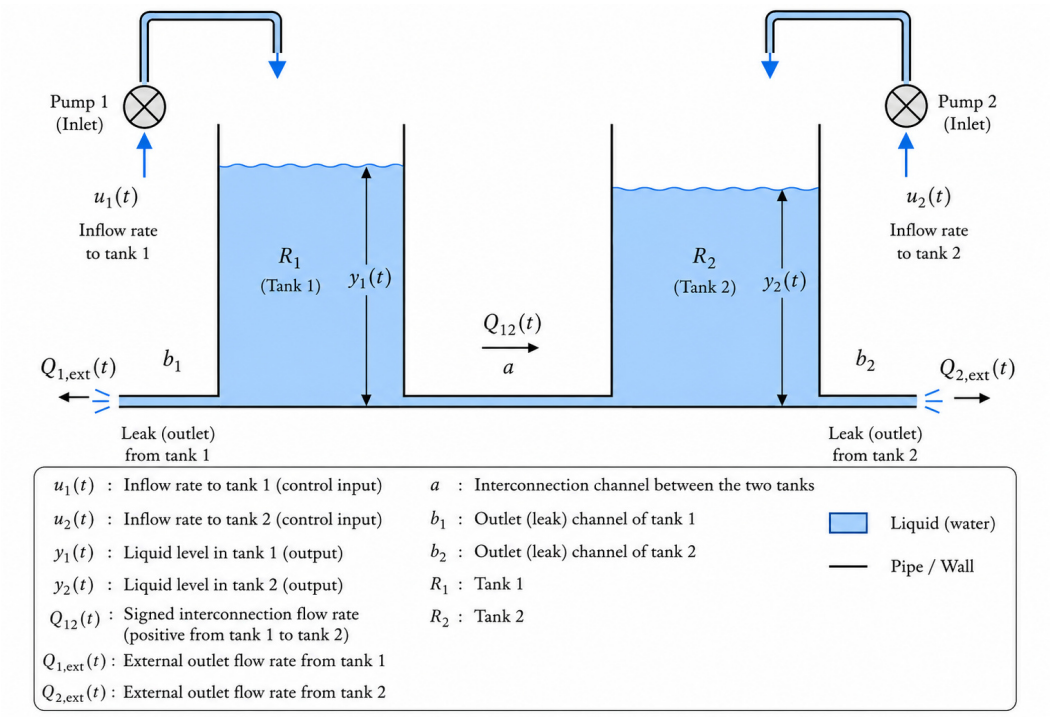



**Figure 1.** Schematic diagram of the interacting two-tank hydraulic system showing the control inputs, interconnection, and external outlet flows.

The system shown in Figure 1 highlights the interconnected nature of the considered process; in particular, any variation in the level $y_1(t)$ may affect the evolution of $y_2(t)$ through the interconnection flow, and conversely.

### *2.2. Modeling Assumptions and Hydraulic Flow Laws*

To derive the mathematical model of the system shown in Figure 1, we adopt the following standard assumptions of hydraulic modeling:

$(H_1)$ The fluid in the tanks is assumed to be incompressible and of constant density.

$(H_2)$ Head losses other than those associated with the flow orifices are neglected.

$(H_3)$ The gravitational acceleration is assumed to be constant and is denoted by $g$, with $g > 0$.

$(H_4)$ The liquid level $y_i(t)$ in each tank $R_i$, $i \in \{1,2\}$, is assumed to be non-negative at every time $t$, that is, $y_i(t) \geq 0$ for $i \in \{1,2\}$.

$(H_5)$ The two tanks $R_1$ and $R_2$ have constant and identical cross-sectional areas, denoted by $A_1$ and $A_2$, respectively, with $A_1 = A_2 = A = 1$, so that the volume variation in each tank can be directly identified with the corresponding level variation.

The flow rates through the orifices are derived from Bernoulli's principle, leading to Torricelli-type relations.

Accordingly, $Q_{12}(t)$ and $Q_{i,\text{ext}}(t)$ describe the passive hydraulic flows shown in Figure 1, whereas $u_i(t)$ represents the externally imposed pump flow.

The interconnection flow rate $Q_{12}(t)$ between tanks $R_1$ and $R_2$ depends, at each time $t$, on the level difference $y_1(t) - y_2(t)$. To fix the sign convention, $Q_{12}(t)$ is defined as a signed flow rate; it is positive for a flow from $R_1$ to $R_2$, i.e., when $y_1(t) > y_2(t)$, and negative for a flow from $R_2$ to $R_1$, i.e., when $y_2(t) > y_1(t)$. It is given by

$$Q_{12}(t) = a \ \text{sign}\left(y_1(t) - y_2(t)\right)\sqrt{2g|y_1(t) - y_2(t)|}. \tag{1}$$

By convention, $Q_{12}(t) = 0$ whenever $y_1(t) = y_2(t)$.

For each tank $R_i$, $i \in \{1,2\}$, the external outlet flow rate $Q_{i,\text{ext}}(t)$ at time $t$ is given by

$$Q_{i,\text{ext}}(t) = b_i\sqrt{2g\, y_i(t)}. \tag{2}$$

Equations (1) and (2) show that both the interconnection flow and the external outlet flows are nonlinear functions of the liquid levels. In particular, the square root dependence and the level difference term introduce nonlinear and coupled hydraulic behavior.

The pump flow $u_i(t)$ is not governed by Equations (1) and (2); it enters directly as a control input in the mass balance equations introduced in the following subsection.

### *2.3. Nonlinear State-Space Model*

The dynamic behavior of the coupled hydraulic system is obtained by applying the mass conservation principle to each tank. According to assumption $(H_5)$, the cross-sectional areas of the two tanks satisfy $A_1 = A_2 = A = 1$. Therefore, the time variation of the liquid volume in each tank is given by $A\dot{y}_i(t)$.

For each tank $R_i$, $i \in \{1,2\}$, the main incoming flow is the supply flow $u_i(t)$, while the external outgoing flow is $Q_{i,\text{ext}}(t)$. The hydraulic exchange between the two tanks is represented by the signed interconnection flow rate $Q_{12}(t)$.

According to the sign convention defined in Equation (1), a positive value of $Q_{12}(t)$ corresponds to a flow from $R_1$ to $R_2$. Therefore, the interconnection flow is subtracted from the mass balance of $R_1$ and added to that of $R_2$. By applying mass conservation to each tank and directly substituting the flow expressions given in Equations (1) and (2), the nonlinear dynamics are obtained as

$$\begin{cases} \dot{y}_1(t) = \dfrac{1}{A}\left(u_1(t) - b_1\sqrt{2g\, y_1(t)} - a \ \text{sign}\big(y_1(t) - y_2(t)\big)\sqrt{2g|y_1(t) - y_2(t)|}\right), \\ \dot{y}_2(t) = \dfrac{1}{A}\left(u_2(t) - b_2\sqrt{2g\, y_2(t)} + a \ \text{sign}\big(y_1(t) - y_2(t)\big)\sqrt{2g|y_1(t) - y_2(t)|}\right). \end{cases} \tag{3}$$

Let the state vector $x(t)$ and the input vector $u(t)$ be defined as

$$x(t) = \begin{pmatrix} x_1(t) \\ x_2(t) \end{pmatrix} = \begin{pmatrix} y_1(t) \\ y_2(t) \end{pmatrix}, \qquad u(t) = \begin{pmatrix} u_1(t) \\ u_2(t) \end{pmatrix}. \tag{4}$$

Since the liquid levels are directly measured, the output vector coincides with the state vector defined in Equation (4), and so is given by

$$Y(t) = x(t). \tag{5}$$

Thus, the nonlinear model (3) can be written in the compact state-space form

$$\begin{cases} \dot{x}(t) = f(x(t)) + \frac{1}{A}u(t), \\ Y(t) = x(t), \end{cases} \tag{6}$$

where $f(x) = \frac{1}{A}\begin{pmatrix} -b_1\sqrt{2g\,x_1} - a\ \mathrm{sign}(x_1 - x_2)\sqrt{2g|x_1 - x_2|} \\ -b_2\sqrt{2g\,x_2} + a\ \mathrm{sign}(x_1 - x_2)\sqrt{2g|x_1 - x_2|} \end{pmatrix}$.

The nonlinear model (6) allows the equilibrium conditions of the system to be characterized. Consider an operating point $x^\star = \begin{pmatrix} y_1^\star \\ y_2^\star \end{pmatrix}$ associated with a constant input $u^\star = \begin{pmatrix} u_1^\star \\ u_2^\star \end{pmatrix}$. At equilibrium, $\dot{x} = 0$, and consequently $f(x^\star) + \frac{1}{A}u^\star = 0$. From the hydraulic model (3), the required equilibrium inflow rates are

$$\begin{cases} u_1^\star = b_1\sqrt{2g\,y_1^\star} + a\ \mathrm{sign}(y_1^\star - y_2^\star)\sqrt{2g|y_1^\star - y_2^\star|}, \\ u_2^\star = b_2\sqrt{2g\,y_2^\star} - a\ \mathrm{sign}(y_1^\star - y_2^\star)\sqrt{2g|y_1^\star - y_2^\star|}. \end{cases} \tag{7}$$

Thus, at equilibrium, the pump inflows balance the external outlet flows and the hydraulic exchange between the two tanks. When $y_1^\star = y_2^\star$, the interconnection flow vanishes and each pump compensates only for the external outlet flow of its corresponding tank.

The nonlinear behavior of system (6) arises from the square root laws governing the interconnection and external outlet flows described by Equations (1) and (2). Consequently, the hydraulic flows depend nonlinearly on the liquid levels, with a sensitivity that varies according to the operating point. In particular, the interconnection flow depends on both the magnitude and the sign of the level difference $y_1 - y_2$, thereby introducing bidirectional coupling between the dynamics of the two tanks. When $y_1 = y_2$, the interconnection flow remains continuous and vanishes, but is not differentiable in the classical sense at this point.

For a regular operating point satisfying $y_1^\star > 0$, $y_2^\star > 0$, and $y_1^\star \neq y_2^\star$, the vector field is differentiable and its Jacobian matrix $J(x^\star)$ is given by

$$J(x^\star) = \frac{1}{A}\begin{pmatrix} -b_1\alpha_1 - a\alpha_{12} & a\alpha_{12} \\ a\alpha_{12} & -b_2\alpha_2 - a\alpha_{12} \end{pmatrix}, \tag{8}$$

where $\alpha_1 = \sqrt{\frac{g}{2y_1^\star}}$, $\alpha_2 = \sqrt{\frac{g}{2y_2^\star}}$, and $\alpha_{12} = \sqrt{\frac{g}{2|y_1^\star - y_2^\star|}}$.

For any nonzero vector $z = \begin{pmatrix} z_1 \\ z_2 \end{pmatrix}$, we obtain

$$z^\top J(x^\star)z = -\frac{1}{A}\left(b_1\alpha_1 z_1^2 + b_2\alpha_2 z_2^2 + a\alpha_{12}(z_1 - z_2)^2\right) < 0. \tag{9}$$

When the leakage cross-sectional areas are strictly positive, the Jacobian matrix is negative definite, which guarantees the local asymptotic stability of the operating point when the inputs are maintained at their equilibrium values. The coupling term attenuates differences between the variations of the two liquid levels, thereby exhibiting a dissipative effect that promotes their equalization.

## 3. Feedback Linearization and Control Design

In this section, we develop the control design strategy for the interacting two-tank hydraulic system. The nonlinear state-space model is first transformed by exact feedback linearization into a control-oriented representation. The theoretical conditions underlying this transformation are explicitly examined through the Lie derivatives, the decoupling matrix, the relative degree, the coordinate transformation, and the zero dynamics. Based on the resulting auxiliary dynamics, PI and PID controllers are then designed and tuned by pole placement. The corresponding closed-loop stability properties are subsequently analyzed for both controller structures.

### *3.1. Feedback Linearization and Control-Oriented Representation*

The nonlinear model given by Equation (6) can be written in control-affine form:

$$\begin{cases} \dot{x}(t) = f(x(t)) + G(x(t))\,u(t), \\ Y(t) = h(x(t)) = x(t), \end{cases} \tag{10}$$

where $G(x) = \frac{1}{A} I_2$. Each control input acts directly on the dynamics of the corresponding state, with the common scaling factor $1/A$ resulting from the identical tank cross-sectional areas.

The state vector $x(t)$ in Equation (10) is the same as that used in Equation (6). Equation (10) is simply the control-affine representation of Equation (6). In this formulation, $I_2$ denotes the $2 \times 2$ identity matrix, while the hydraulic coupling remains contained in the nonlinear vector field $f(x)$.

Due to the square root terms in the interconnection and external outlet flow laws given by Equations (1) and (2), the vector field $f(x)$ is not differentiable over the entire physical domain. The differential analysis required for feedback linearization is carried out over the regular domain

$$\Omega = \left\{ x = \begin{pmatrix} x_1 \\ x_2 \end{pmatrix} \in \mathbb{R}^2 : x_1 > 0,\ x_2 > 0,\ x_1 \neq x_2 \right\}. \tag{11}$$

On the domain $\Omega$, the vector field $f(x)$ is differentiable. The output functions are $h_1(x) = x_1$ and $h_2(x) = x_2$. Denoting $g_1 = \begin{pmatrix} 1/A \\ 0 \end{pmatrix}$ and $g_2 = \begin{pmatrix} 0 \\ 1/A \end{pmatrix}$ as the columns of $G(x)$, the first time derivative of each output is written as

$$\dot{Y}_i = L_f h_i(x) + \sum_{j=1}^{2} L_{g_j} h_i(x)\, u_j, \qquad i = 1, 2. \tag{12}$$

The Lie derivatives are defined by $L_f h_i(x) = \nabla h_i(x)^\top f(x)$ and $L_{g_j} h_i(x) = \nabla h_i(x)^\top g_j(x)$. Since $h_i(x) = x_i$, we obtain $L_f h_i(x) = f_i(x)$ and $L_{g_j} h_i(x) = \frac{1}{A}\delta_{ij}$, where $\delta_{ij} = \begin{cases} 1 & \text{if } i = j; \\ 0 & \text{if } i \neq j \end{cases}$ denotes the Kronecker delta.

Therefore, the decoupling matrix is

$$\mathcal{A}(x) = \begin{pmatrix} L_{g_1}h_1 & L_{g_2}h_1 \\ L_{g_1}h_2 & L_{g_2}h_2 \end{pmatrix} = \frac{1}{A}\begin{pmatrix} 1 & 0 \\ 0 & 1 \end{pmatrix} = \frac{1}{A}I_2. \tag{13}$$

Since the decoupling matrix is nonsingular, with $\det(\mathcal{A}(x)) = \frac{1}{A^2} > 0$, each output has relative degree one; therefore, the relative-degree vector is $(r_1, r_2) = (1, 1)$ and the total relative degree satisfies $r_1 + r_2 = 2 = n$, where $n = 2$ is the dimension of the system. Since the total relative degree is equal to the state dimension, no internal dynamics remain after linearization, so the zero dynamics are of zero dimension.

The coordinate transformation associated with the outputs is defined by

$$\xi = \Phi(x) = \begin{pmatrix} h_1(x) \\ h_2(x) \end{pmatrix} = \begin{pmatrix} x_1 \\ x_2 \end{pmatrix} = x. \tag{14}$$

Its Jacobian is $\frac{\partial \Phi(x)}{\partial x} = I_2$, and as such is nonsingular. The transformation $\Phi$ is a diffeomorphism, and in the present case, the linearizing coordinates $\xi$ directly coincide with the original state coordinates; together with the nonsingularity of the decoupling matrix and the full relative degree established above, these properties satisfy the conditions required for exact feedback linearization over the regular domain $\Omega$.

We then introduce the auxiliary input

$$v(t) = \begin{pmatrix} v_1(t) \\ v_2(t) \end{pmatrix}. \tag{15}$$

For a multivariable system with relative degree $(1, 1)$, the input–output feedback linearization law is written as

$$u(t) = \mathcal{A}(x(t))^{-1}\Big(v(t) - L_f h(x(t))\Big), \tag{16}$$

where $L_f h(x) = \big(L_f h_1(x), L_f h_2(x)\big)^\top$.

For the considered system, $\mathcal{A}(x) = \frac{1}{A}I_2$ and $L_f h(x) = f(x)$. Therefore, the control law reduces to

$$u(t) = A(v(t) - f(x(t))). \tag{17}$$

Substituting (17) into the nonlinear model (6), the nonlinear hydraulic terms are exactly compensated and the transformed dynamics become

$$\begin{cases} \dot{x}(t) = v(t), \\ Y(t) = x(t). \end{cases} \tag{18}$$

Since $\xi = x$, this relation can also be written as $\dot{\xi}(t) = v(t)$. Therefore, the two control channels are decoupled in the linearized dynamics, with

$$\begin{cases} \dot{y}_1(t) = v_1(t), \\ \dot{y}_2(t) = v_2(t). \end{cases} \tag{19}$$

Returning to the physical inputs applied to the pumps, we obtain

$$\begin{cases} u_1(t) &= b_1\sqrt{2g\,y_1(t)} + a\ \mathrm{sign}\big(y_1(t) - y_2(t)\big)\sqrt{2g\,|y_1(t) - y_2(t)|} + Av_1(t), \\ u_2(t) &= b_2\sqrt{2g\,y_2(t)} - a\ \mathrm{sign}\big(y_1(t) - y_2(t)\big)\sqrt{2g\,|y_1(t) - y_2(t)|} + Av_2(t). \end{cases} \tag{20}$$

Thus, the law in (17) achieves exact compensation of the hydraulic nonlinearities within the nominal model. This compensation assumes that the parameters $A$, $a$, $b_1$, $b_2$, and $g$ are known and that the liquid levels $y_1(t)$ and $y_2(t)$ are available for state feedback. The differential conditions used in the preceding analysis are established over the regular domain $\Omega$. When $y_1 = y_2$, the interconnection flow remains continuous and vanishes, but is not differentiable in the classical sense. However, under the convention $\operatorname{sign}(0) = 0$, the compensation law (17) remains algebraically well-defined on this surface. The auxiliary inputs $v_1(t)$ and $v_2(t)$ can then be designed using linear control laws, in particular PI or PID controllers.

### *3.2. PI and PID Controller Design, Tuning, and Stability*

Following feedback linearization, the auxiliary input–output dynamics are given by Equation (19). Therefore, the controllers can be designed on the linearized channels, while the physical control inputs applied to the pumps are obtained through the nonlinear compensation law given by Equation (20). This provides a clear separation between the design of the auxiliary linear control laws and their implementation on the original nonlinear hydraulic system.

Let $y_{i,\mathrm{ref}}(t)$, $i \in \{1,2\}$, denote the desired reference level for tank $R_i$. The tracking error $e_i(t)$ is defined as

$$e_i(t) = y_{i,\mathrm{ref}}(t) - y_i(t), \qquad i \in \{1,2\}. \tag{21}$$

The objective of the controller is to generate the auxiliary input $v_i(t)$ such that the liquid level $y_i(t)$ tracks the reference $y_{i,\mathrm{ref}}(t)$.

In the following, the reference levels are assumed to be constant, so that $\dot{y}_{i,\mathrm{ref}}(t) = 0$. Using the auxiliary dynamics (19), the tracking error dynamics then satisfy

$$\dot{e}_i(t) = -\dot{y}_i(t) = -v_i(t), \qquad i \in \{1,2\}. \tag{22}$$

In this study, the analysis is deliberately restricted to PI and PID architectures. In particular, these two conventional control structures allow us to examine the effect of introducing a derivative action while retaining a common design basis. Within this framework, the PI and PID controllers are not applied directly to the original nonlinear hydraulic model; instead, they are designed for the linearized auxiliary dynamics (19). The physical control inputs applied to the pumps are then obtained by substituting $v_1(t)$ and $v_2(t)$ into the nonlinear compensation law (20). Thus, the nonlinear compensation accounts for the hydraulic nonlinearities, whereas the PI and PID control laws determine the tracking behavior of the two liquid levels.

The gains of the PI and PID controllers are determined using a tuning procedure based on pole placement, which is applied to the linearized auxiliary dynamics.

For both control structures, the same tuning principle is applied to the two loops $i \in \{1,2\}$. A common parameter $\lambda > 0$ is introduced to impose the same real part, which is equal to $-\lambda$, on the closed-loop poles. This parameter determines a common nominal exponential decay rate for the PI- and PID-controlled dynamics. In addition, a distinct damping ratio is introduced for each controller structure: the PI controller is characterized by $0 < \zeta^{\mathrm{PI}} \leq 1$, whereas the PID controller is characterized by $0 < \zeta^{\mathrm{PID}} < 1$. For each structure, the corresponding damping ratio determines the pole configuration, while the common parameter $\lambda$ preserves the same pole real part $-\lambda$.

A sensitivity analysis is conducted in Section 5.2 to evaluate the influence of the tuning parameters $\lambda$, $\zeta^{\mathrm{PI}}$, and $\zeta^{\mathrm{PID}}$ on the closed-loop time-domain performance. In the numerical study presented in Section 5, the nominal tuning parameters are set to $\lambda = 1$, $\zeta^{\mathrm{PI}} = 1$,

and $\zeta^{\mathrm{PID}} = 1/\sqrt{2}$. These values define the baseline controller configurations used in the subsequent analyses.

#### 3.2.1. PI Controller

For a PI controller, the auxiliary input is chosen as

$$v_i(t) = K_{P_i}^{\mathrm{PI}} e_i(t) + K_{I_i}^{\mathrm{PI}} \int_0^t e_i(\tau)\, d\tau, \qquad i \in \{1,2\}. \tag{23}$$

Using the error dynamics (22), the characteristic polynomial $P_{\mathrm{PI},i}$ associated with each loop $i \in \{1,2\}$ is written as

$$P_{\mathrm{PI},i}(s) = s^2 + K_{P_i}^{\mathrm{PI}} s + K_{I_i}^{\mathrm{PI}}. \tag{24}$$

To obtain closed-loop dynamics with an adjustable damping ratio, the desired polynomial is chosen as

$$P_{\mathrm{PI},i}^{d}(s) = s^2 + 2\lambda s + \frac{\lambda^2}{(\zeta^{\mathrm{PI}})^2}, \qquad \lambda > 0, \quad 0 < \zeta^{\mathrm{PI}} \leq 1. \tag{25}$$

Matching the coefficients of (24) and (25) then yields the controller gains

$$\begin{cases} K_{P_i}^{\mathrm{PI}} = 2\lambda, \\ K_{I_i}^{\mathrm{PI}} = \dfrac{\lambda^2}{(\zeta^{\mathrm{PI}})^2}, \end{cases} \qquad i \in \{1,2\}. \tag{26}$$

For each loop, the two poles of the characteristic polynomial are $s_{1,2} = -\lambda \pm j\lambda\sqrt{\frac{1}{(\zeta^{\mathrm{PI}})^2} - 1}$. For $\lambda > 0$ and $0 < \zeta^{\mathrm{PI}} < 1$, the poles form a complex-conjugate pair with real part equal to $-\lambda$, corresponding to an underdamped regime. When $\zeta^{\mathrm{PI}} = 1$, the two poles coincide at $s_{1,2} = -\lambda$, corresponding to critical damping. Therefore, for $0 < \zeta^{\mathrm{PI}} \leq 1$, all closed-loop poles lie strictly in the open left-half complex plane, which guarantees the asymptotic stability of the nominal error dynamics controlled by the PI controller.

#### 3.2.2. PID Controller

For a PID controller, the auxiliary input is chosen as

$$v_i(t) = K_{P_i}^{\mathrm{PID}} e_i(t) + K_{I_i}^{\mathrm{PID}} \int_0^t e_i(\tau)\, d\tau + K_{D_i}^{\mathrm{PID}} \dot{e}_i(t), \qquad i \in \{1,2\}. \tag{27}$$

Using the error dynamics (22) and differentiating the resulting closed-loop equation with respect to time, the characteristic polynomial $P_{\mathrm{PID},i}$ associated with each loop $i \in \{1,2\}$ is written as

$$P_{\mathrm{PID},i}(s) = \left(1 + K_{D_i}^{\mathrm{PID}}\right) s^2 + K_{P_i}^{\mathrm{PID}} s + K_{I_i}^{\mathrm{PID}}. \tag{28}$$

To prescribe a pole real part equal to $-\lambda$ while allowing the damping of the PID-controlled dynamics to be adjusted through $\zeta^{\mathrm{PID}}$, the desired characteristic polynomial is chosen as

$$P_{\mathrm{PID},i}^{d}(s) = s^2 + 2\lambda s + \frac{\lambda^2}{(\zeta^{\mathrm{PID}})^2}, \qquad 0 < \zeta^{\mathrm{PID}} < 1. \tag{29}$$

After normalizing (28), matching its coefficients with those of (29) yields

$$\begin{cases} \dfrac{K_{P_i}^{\mathrm{PID}}}{1+K_{D_i}^{\mathrm{PID}}} = 2\lambda, \\ \dfrac{K_{I_i}^{\mathrm{PID}}}{1+K_{D_i}^{\mathrm{PID}}} = \dfrac{\lambda^2}{\left(\zeta^{\mathrm{PID}}\right)^2}. \end{cases} \tag{30}$$

The two relations (30) ensure the prescribed pole placement but leave one degree of freedom, since the PID controller contains three gains. To determine this remaining degree of freedom without introducing an additional tuning parameter, the numerator of the PID controller is chosen to have two coincident real zeros. This condition corresponds to setting its discriminant equal to zero, and is written as

$$\left(K_{P_i}^{\mathrm{PID}}\right)^2 = 4K_{D_i}^{\mathrm{PID}}K_{I_i}^{\mathrm{PID}}. \tag{31}$$

Combining relations (30) and (31) then yields the PID controller gains in the form

$$\begin{cases} K_{D_i}^{\mathrm{PID}} = \dfrac{\left(\zeta^{\mathrm{PID}}\right)^2}{1-\left(\zeta^{\mathrm{PID}}\right)^2}, \\ K_{P_i}^{\mathrm{PID}} = \dfrac{2\lambda}{1-\left(\zeta^{\mathrm{PID}}\right)^2}, \\ K_{I_i}^{\mathrm{PID}} = \dfrac{\lambda^2}{\left(\zeta^{\mathrm{PID}}\right)^2\left(1-\left(\zeta^{\mathrm{PID}}\right)^2\right)}. \end{cases} \qquad i \in \{1,2\}. \tag{32}$$

For each loop, the two poles of the characteristic polynomial are then $s_{1,2} = -\lambda \pm j\lambda\sqrt{\frac{1}{\left(\zeta^{\mathrm{PID}}\right)^2}-1}$. Since $\lambda > 0$ and $0 < \zeta^{\mathrm{PID}} < 1$, the poles form a complex-conjugate pair with real part equal to $-\lambda$, corresponding to an underdamped regime. Therefore, both poles lie strictly in the open left-half complex plane, which guarantees the asymptotic stability of the nominal error dynamics controlled by the PID controller. The parameter $\zeta^{\mathrm{PID}}$ determines the damping characteristics of the closed-loop dynamics, while $\lambda$ preserves the prescribed pole real part $-\lambda$.

## 4. Game-Theoretic Controller Selection Framework

In this section, we use tools from non-cooperative game theory to address the controller structure selection problem for the coupled hydraulic system. Each tank $R_i$, $i \in \{1,2\}$, is associated with a decision-maker $\mathcal{P}_i$ that selects a controller structure $s_i$ from its strategy set $S_i$, given by

$$S_i = \{\mathrm{PI}, \mathrm{PID}\}. \tag{33}$$

The choice $s_i \in S_i$ made by decision-maker $\mathcal{P}_i$ cannot be analyzed independently of the choice $s_{-i}$ made by the other decision-maker $\mathcal{P}_{-i}$, since the two tanks are coupled through the hydraulic flow between $R_1$ and $R_2$. Therefore, the strategy selected for one control loop may influence the control effort required in the neighboring loop.

This interdependence persists at the level of the physical control inputs despite the decoupling of the auxiliary dynamics achieved by exact feedback linearization. Indeed, for fixed tuning parameters, the choice $s_i$ determines the auxiliary control law $v_i(t)$, which directly contributes to the physical input $u_i(t)$ and governs the evolution of the liquid level $y_i(t)$. Likewise, the choice $s_{-i}$ of the neighboring loop determines $v_{-i}(t)$ and consequently the evolution of $y_{-i}(t)$. The two level trajectories $y_i(t)$ and $y_{-i}(t)$ then enter the hydraulic coupling term of the nonlinear compensation law (20). Consequently, the control energy cost $J_i$ depends on the complete strategy profile $(s_i, s_{-i})$. This cross-dependence between

the controller structure decisions and the resulting costs constitutes the strategic interaction that motivates the game-theoretic formulation of the selection problem.

Within this framework, the decision criterion considered for each decision-maker is the control effort required by the corresponding pump. Thus, for each decision-maker $\mathcal{P}_i$, the cost function $J_i$ is defined as the control energy associated with the physical input signal $u_i(t)$:

$$J_i(s_i, s_{-i}) = \int_0^T u_i^2(t; s_i, s_{-i})\, dt, \qquad i \in \{1, 2\} \tag{34}$$

where $T > 0$ denotes the simulation horizon, $s_i$ represents the strategy selected by decision-maker $\mathcal{P}_i$, and $s_{-i}$ denotes the strategy selected by the other decision-maker. The tuning parameters $\lambda$, $\zeta^{\mathrm{PI}}$, and $\zeta^{\mathrm{PID}}$ are kept fixed during each game evaluation.

The adopted controller selection game is non-cooperative. Each decision-maker independently minimizes the control energy cost associated with its corresponding pump. The game is also static because the choice between a PI and a PID structure is treated as a design decision made once before operation, after which the selected structure is kept fixed throughout the evaluation horizon. Although the hydraulic states and control inputs evolve dynamically over time, the controller structure decision itself remains unchanged. Moreover, each decision-maker evaluates their available strategies according to a single criterion consisting of the control energy required by its actuator. Because this is directly related to the physical control effort, it provides a clear and consistent basis for comparing different combinations of controller structure.

### *4.1. Normal-Form Formulation of the Static Game*

The interaction between the decisions of the two decision-makers $\mathcal{P}_1$ and $\mathcal{P}_2$ can be formulated as a static non-cooperative game in normal form. The static nature of the game means that the two decision-makers simultaneously select their controller structures only once, before the closed-loop behavior of the system is evaluated; therefore, each decision-maker selects a strategy without observing the strategy selected by the other.

Let $\mathcal{N} = \{\mathcal{P}_1, \mathcal{P}_2\}$ denote the set of players. The static game in normal form is then described by the triplet

$$\mathcal{G} = \left\langle \mathcal{N},\ (S_i)_{i\in\{1,2\}}, (J_i)_{i\in\{1,2\}} \right\rangle, \tag{35}$$

where $S_i = \{\mathrm{PI}, \mathrm{PID}\}$ denotes the strategy set of player $\mathcal{P}_i$ and $J_i$ denotes the cost function incurred by player $\mathcal{P}_i$ in controlling tank $R_i$.

Since each player has two available strategies, the set of admissible strategy profiles is

$$S_1 \times S_2 = \{(\mathrm{PI}, \mathrm{PI}), (\mathrm{PI}, \mathrm{PID}), (\mathrm{PID}, \mathrm{PI}), (\mathrm{PID}, \mathrm{PID})\}. \tag{36}$$

For each strategy profile, the costs $J_1$ and $J_2$ are computed from the physical control inputs applied to the two pumps. These costs can be organized in a cost bimatrix. The rows correspond to the strategies of player $\mathcal{P}_1$, whereas the columns correspond to the strategies of player $\mathcal{P}_2$. Each entry contains the pair of costs obtained for the corresponding strategy profile:

$$\begin{array}{cc} & \begin{array}{cc} \multicolumn{2}{c}{\mathcal{P}_2} \\ \mathrm{PI} & \mathrm{PID} \end{array} \\ \begin{array}{c} \mathcal{P}_1 \\ \\ \end{array} & \begin{array}{c} \mathrm{PI} \\ \mathrm{PID} \end{array} \begin{pmatrix} (J_1^{11}, J_2^{11}) & (J_1^{12}, J_2^{12}) \\ (J_1^{21}, J_2^{21}) & (J_1^{22}, J_2^{22}) \end{pmatrix} \end{array} \tag{37}$$

where $J_i^{kl}$ denotes the cost of player $\mathcal{P}_i$, $i \in \{1, 2\}$, when $\mathcal{P}_1$ selects their $k$-th strategy and $\mathcal{P}_2$ selects their $l$-th strategy, with $k, l \in \{1, 2\}$. In this notation, the indices $k$ and $l$ identify

the strategies selected by $\mathcal{P}_1$ and $\mathcal{P}_2$, respectively. For both indices, the value 1 corresponds to the PI strategy, whereas the value 2 corresponds to the PID strategy.

### *4.2. Nash Equilibrium Characterization*

Since the entries of the bimatrix (37) represent costs, each player $\mathcal{P}_i$, $i \in \{1,2\}$, seeks to minimize their own cost function. Thus, a strategy profile $s^\star = (s_1^\star, s_2^\star) \in S_1 \times S_2$ is a Nash equilibrium if no player can reduce their cost by unilaterally changing their own strategy while the strategy of the other player remains unchanged.

Using the indexed notation of the cost bimatrix, a profile $(s_1^{k^\star}, s_2^{l^\star})$, $k^\star, l^\star \in \{1,2\}$ is a Nash equilibrium if and only if

$$\begin{cases} J_1^{k^\star l^\star} \leq J_1^{k l^\star}, & \forall k \in \{1,2\}, \\ J_2^{k^\star l^\star} \leq J_2^{k^\star l}, & \forall l \in \{1,2\}. \end{cases} \tag{38}$$

In this notation, index 1 corresponds to the PI strategy, whereas index 2 corresponds to the PID strategy.

The following proposition establishes the existence properties of Nash equilibria for the controller selection game $\mathcal{G}$ defined in Equation (35).

**Proposition 1.** *Consider the controller structure selection game $\mathcal{G}$ and its associated cost bimatrix given by Equation (37). Assume that the costs $J_i(s_1, s_2)$ are well-defined and finite for every strategy profile $(s_1, s_2) \in S_1 \times S_2$. Then:*

*(i) The game $\mathcal{G}$ admits at least one Nash equilibrium in mixed strategies.*

*(ii) The game $\mathcal{G}$ admits a Nash equilibrium in pure strategies if and only if there exists $(k^\star, l^\star) \in \{1,2\}^2$ satisfying the two conditions in Equation (38). In this case, the strategy profile $(s_1^{k^\star}, s_2^{l^\star})$ constitutes a pure-strategy Nash equilibrium of $\mathcal{G}$.*

**Proof.** For statement (i), the game $\mathcal{G}$ consists of two players, so that $|\mathcal{N}| = 2 < \infty$. Moreover, each player $\mathcal{P}_i$ has the strategy set $S_i = \{\text{PI}, \text{PID}\}$; therefore, $|S_i| = 2 < \infty$, $i \in \{1,2\}$. Thus, $\mathcal{G}$ is a finite bimatrix game. According to Nash's existence theorem, every finite game admits at least one Nash equilibrium in mixed strategies [20]. This proves statement (i).

For statement (ii), suppose first that $(s_1^{k^\star}, s_2^{l^\star})$ is a pure-strategy Nash equilibrium. By definition, neither player can decrease its cost by unilaterally changing its own strategy. Therefore, the two inequalities in Equation (38) necessarily hold. Conversely, if there exists $(k^\star, l^\star) \in \{1,2\}^2$ satisfying both inequalities in Equation (38), then $s_1^{k^\star}$ is a best response to $s_2^{l^\star}$ and $s_2^{l^\star}$ is a best response to $s_1^{k^\star}$. Hence, the two strategies are mutual best responses, and $(s_1^{k^\star}, s_2^{l^\star})$ constitutes a pure-strategy Nash equilibrium of $\mathcal{G}$. □

### *4.3. Numerical Procedure for Nash Equilibrium Identification*

To study the evolution of the Nash equilibrium with respect to the physical parameters, the procedure evaluates each strategy profile, simulates the closed-loop system, computes the pump control inputs and associated costs, evaluates the time-domain performance indicators, and constructs the cost bimatrix used to identify the Nash equilibria.

Although Proposition 1 guarantees the existence of a Nash equilibrium in the mixed-strategy extension, this study focuses on pure-strategy equilibria, consistent with the deterministic assignment of a PI or PID controller to each control loop.

The computational complexity of Algorithm 1 is mainly determined by the numerical simulations. Each admissible strategy profile requires a closed-loop simulation. The game $\mathcal{G}$, defined by Equation (35), is a finite two-player game in which each player has two available strategies. Consequently, only $2^2 = 4$ strategy profiles need to be evaluated.

**Algorithm 1** Procedure for identifying the Nash equilibrium and evaluating time-domain performance

**Inputs:** $g$, $A$, $a$, $b_1$, $b_2$, $\lambda$, $\zeta^{\mathrm{PI}}$, $\zeta^{\mathrm{PID}}$, $T$, $\Delta t$, $y_1(0)$, $y_2(0)$, $y_{1,\mathrm{ref}}$, and $y_{2,\mathrm{ref}}$.
Define the set of strategy profiles:
$S_1 \times S_2 = \{(\mathrm{PI},\mathrm{PI}), (\mathrm{PI},\mathrm{PID}), (\mathrm{PID},\mathrm{PI}), (\mathrm{PID},\mathrm{PID})\}$.
**for** each strategy profile $s = (s_1, s_2) \in S_1 \times S_2$ **do**
  **for** each player $\mathcal{P}_i$, $i \in \{1,2\}$ **do**
    **if** $s_i = \mathrm{PI}$ **then**
      Compute $K_{P_i}^{\mathrm{PI}}$ and $K_{I_i}^{\mathrm{PI}}$ using (26).
    **else if** $s_i = \mathrm{PID}$ **then**
      Compute $K_{P_i}^{\mathrm{PID}}$, $K_{I_i}^{\mathrm{PID}}$, and $K_{D_i}^{\mathrm{PID}}$ using (32).
    **end if**
  **end for**
  Reset the system states to the initial conditions $y_1(0)$ and $y_2(0)$.
  Reset the controller integral states $\eta_i(0) = 0$, $i \in \{1,2\}$, where $\eta_i(t) = \int_0^t e_i(\tau)\, d\tau$.
  **for** each time step $t_k \in [0, T]$ **do**
    Compute $e_1(t_k)$ and $e_2(t_k)$ using (21).
    **for** each player $\mathcal{P}_i$, $i \in \{1,2\}$ **do**
      **if** $s_i = \mathrm{PI}$ **then**
        Compute $v_i(t_k)$ using the PI control law given by (23).
      **else if** $s_i = \mathrm{PID}$ **then**
        Using (22) and (27), compute $v_i(t_k) = \dfrac{K_{P_i}^{\mathrm{PID}} e_i(t_k) + K_{I_i}^{\mathrm{PID}} \eta_i(t_k)}{1 + K_{D_i}^{\mathrm{PID}}}$.
      **end if**
    **end for**
    Compute the unconstrained physical control input $u_i^{\mathrm{unc}}(t_k)$, $i \in \{1,2\}$, from (20).
    Apply $u_i(t_k) = \max\{0, u_i^{\mathrm{unc}}(t_k)\}$, $i \in \{1,2\}$.
    Update $y_1(t_{k+1})$ and $y_2(t_{k+1})$ using the nonlinear model (3).
    Update the controller integral states according to $\dot{\eta}_i(t) = e_i(t)$, $i \in \{1,2\}$.
  **end for**
  Compute $J_1(s_1, s_2)$ and $J_2(s_1, s_2)$ using (34).
  **for** each player $\mathcal{P}_i$, $i \in \{1,2\}$ **do**
    Compute: $M_{p,i} = \begin{cases} 100 \dfrac{\max_{t\in[0,T]}\{0,\ \mathrm{sign}(y_{i,\mathrm{ref}} - y_i(0))\,(y_i(t) - y_{i,\mathrm{ref}})\}}{|y_{i,\mathrm{ref}} - y_i(0)|}, & y_{i,\mathrm{ref}} \neq y_i(0), \\ 0, & y_{i,\mathrm{ref}} = y_i(0). \end{cases}$
    Compute: $T_{s,i} = \inf\{t \in [0,T] : |y_i(\tau) - y_{i,\mathrm{ref}}| \leq 0.02|y_{i,\mathrm{ref}}|,\ \forall\, \tau \in [t,T]\}$.
    Compute: $e_{ss,i} \simeq |e_i(T)| = |y_{i,\mathrm{ref}} - y_i(T)|$.
  **end for**
**end for**
Construct the cost bimatrix given by (37) from the four strategy profiles.
Identify the pure-strategy Nash equilibrium profiles using the conditions in (38).
**Outputs:** cost bimatrix, pure-strategy Nash equilibrium profiles, and the performance indicators: maximum overshoot $M_{p,i}$, settling time $T_{s,i}$, and finite-horizon steady-state error $e_{ss,i}$, for each player $\mathcal{P}_i$, $i \in \{1,2\}$, and each strategy profile $s = (s_1, s_2)$.

Let $N_T = \frac{T}{\Delta t}$ denote the number of simulation steps. For each profile, the evaluation of the control laws, computation of the physical control inputs, state update, and cost evaluation require a constant number of operations at each time step. Therefore, the computational complexity of simulating one profile is $O(N_T)$, leading to an overall complexity of $O(4N_T) = O(N_T)$ for the four profiles. Once the cost bimatrix has been constructed, the pure-strategy Nash equilibria are identified by checking mutual best responses. Since the game $\mathcal{G}$ contains only four strategy profiles, this verification has complexity $O(1)$.

More generally, for a game with $n$ players, each having $m$ available strategies, the number of strategy profiles is $m^n$. Their exhaustive evaluation requires $O(m^n N_T)$ operations, whereas the identification of best responses from the cost tensor can be performed in $O(nm^n)$. Thus, the overall complexity is $O(m^n N_T + nm^n)$, with $O(m^n N_T)$ being the dominant term when $N_T$ is large compared with $n$.

## 5. Numerical Results and Discussion

### *5.1. Reference Configuration and Nominal Results*

This first numerical study establishes the reference configuration. Algorithm 1 is applied with the common parameters $g = 9.81$, $\lambda = 1$, $\zeta^{\mathrm{PI}} = 1$, $\zeta^{\mathrm{PID}} = \frac{1}{\sqrt{2}}$, $T = 20$, $\Delta t = 10^{-3}$, together with the constant reference levels $y_{1,\mathrm{ref}} = y_{2,\mathrm{ref}} = 1$.

For the physical parameters and initial conditions, we adopt the following reference configuration: $a = 0.1$, $A = 1$, $b_1 = b_2 = 0.60$, $y_1(0) = y_2(0) = 0.10$.

This configuration is fully symmetric with respect to the two tanks. It is used as a reference point to analyze changes in the Nash equilibrium structure when the tuning parameters are modified (as investigated in Section 5.2) or when the physical parameters and operating conditions are varied (as examined in Section 5.3) while keeping the remaining parameters constant.

The resulting cost bimatrix for this reference configuration is shown below.

$$\begin{array}{cc} & \begin{array}{cc} \multicolumn{2}{c}{\mathcal{P}_2} \\ \mathrm{PI} & \mathrm{PID} \end{array} \\ \begin{array}{c} \mathcal{P}_1 \\ \\ \end{array} \begin{array}{c} \mathrm{PI} \\ \mathrm{PID} \end{array} & \begin{pmatrix} (145.7067, 145.7067) & (146.4926, 145.3095) \\ (145.3095, 146.4926) & (\mathbf{145.9092}, \mathbf{145.9092}) \end{pmatrix} \end{array} \tag{39}$$

According to the Nash equilibrium criterion given by Equation (38), the unique equilibrium associated with this bimatrix is the symmetric profile $(\mathrm{PID}, \mathrm{PID})$.

This result reflects a mechanism that goes beyond a simple comparison of the numerical costs. Although feedback linearization decouples the auxiliary tracking dynamics, the hydraulic interaction remains present in the physical control inputs through the interconnection flow between the tanks. Thus, the controller selected for one loop affects not only its own control effort but also the control effort required by the neighboring loop. The resulting equilibrium arises from a trade-off between the intrinsic dynamic properties of the PI and PID structures and their interaction through the physical coupling of the process.

The comparison with the $(\mathrm{PI}, \mathrm{PI})$ profile also shows that strategic stability does not necessarily coincide with the minimization of the overall energy cost. Although this profile yields a lower total cost, each player can individually reduce their own cost by changing their strategy. Therefore, the $(\mathrm{PID}, \mathrm{PID})$ profile emerges not as a collective energy optimum but as a configuration that is stable against unilateral deviations.

To complement the energy-cost-based analysis, three time-domain performance indicators are evaluated for each player $\mathcal{P}_i$, $i \in \{1, 2\}$, and each strategy profile $(s_1, s_2) \in S_1 \times S_2$: the maximum overshoot $M_{p,i}$, the settling time $T_{s,i}$ within a $\pm 2\%$ band around the reference, and the finite-horizon approximation of the steady-state error $e_{ss,i} \simeq |e_i(T)|$. The results obtained for $T = 20$ s are reported in Table 1.

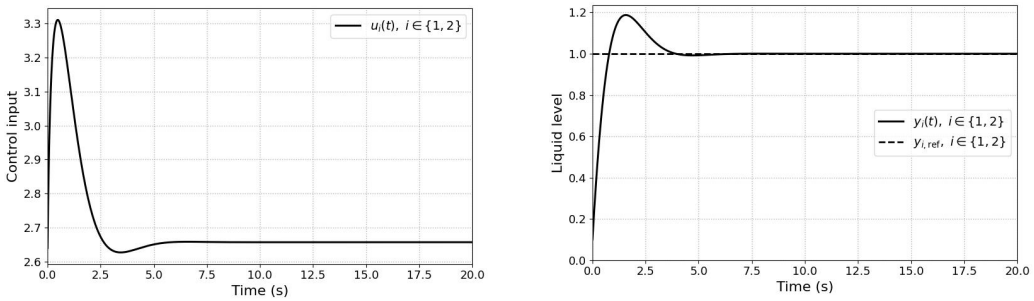
Table 1 highlights two distinct dynamic behaviors. A PI-controlled loop exhibits a maximum overshoot of 13.55%, a settling time of 5.253 s, and a residual error at $T = 20$ s of approximately $3.49 \times 10^{-8}$, whereas with PID these values become 20.82%, 3.422 s, and $9.85 \times 10^{-10}$, respectively. Thus, the PID controller reduces the settling time by approximately 34.9% and yields a significantly lower residual error, at the cost of an approximately 53.7% increase in overshoot. These results reveal a trade-off between convergence speed, accuracy, and transient overshoot.

**Table 1.** Time-domain performance indicators for the four strategy profiles in the nominal configuration.

| $s = (s_1, s_2)$ | $\mathcal{P}_1$ | | | $\mathcal{P}_2$ | | |
|---|---|---|---|---|---|---|
| | $M_{p,1}$ (%) | $T_{s,1}$ (s) | $e_{ss,1}$ | $M_{p,2}$ (%) | $T_{s,2}$ (s) | $e_{ss,2}$ |
| (PI, PI) | 13.5471 | 5.253 | $3.49 \times 10^{-8}$ | 13.5471 | 5.253 | $3.49 \times 10^{-8}$ |
| (PI, PID) | 13.5471 | 5.253 | $3.49 \times 10^{-8}$ | 20.8207 | 3.422 | $9.85 \times 10^{-10}$ |
| (PID, PI) | 20.8207 | 3.422 | $9.85 \times 10^{-10}$ | 13.5471 | 5.253 | $3.49 \times 10^{-8}$ |
| (PID, PID) | 20.8207 | 3.422 | $9.85 \times 10^{-10}$ | 20.8207 | 3.422 | $9.85 \times 10^{-10}$ |

The repetition of the same values for a given controller structure across different strategy profiles follows directly from the closed-loop model structure. When the non-negativity constraint is inactive, exact feedback linearization leads to the decoupled auxiliary dynamics $\dot{y}_i = v_i$; therefore, the time-domain performance indicators of each loop are determined by its own PI or PID structure. In contrast, the energy costs $J_i$ remain dependent on the complete strategy profile $(s_1, s_2)$, since the physical control inputs given by Equation (20) retain the hydraulic coupling term. The time-domain indicators characterize the dynamic consequences of each strategy, whereas the energy cost remains the sole criterion used to determine the Nash equilibrium.

To illustrate the system behavior at the Nash equilibrium profile (PID, PID), Figure 2 presents the physical control inputs $u_i(t)$ and the liquid levels $y_i(t)$, $i \in \{1, 2\}$, for the nominal configuration.




(**a**) Physical control inputs $u_i(t)$, $i \in \{1, 2\}$. (**b**) Liquid level responses $y_i(t)$, $i \in \{1, 2\}$.

**Figure 2.** Closed-loop time responses of the system in the nominal configuration with the Nash equilibrium profile (PID, PID).

In this symmetric configuration with the (PID, PID) controller profile, the physical parameters, initial conditions, and reference levels are identical for the two tanks. By symmetry, $y_1(t) = y_2(t)$; therefore, $Q_{12}(t) = 0$ and $u_1(t) = u_2(t)$. Consequently, the trajectories of the two loops overlap in Figure 2. The numerical verification also shows that the unconstrained control inputs $u_i^{\mathrm{unc}}$ remain positive over the entire simulation horizon. Therefore, the non-negativity constraint introduced in Algorithm 1 is inactive in this nominal configuration.

Figure 2b confirms convergence to the reference level and the transient behavior quantified in Table 1. The 20.82% overshoot associated with the PID controller is non-negligible, but does not indicate instability because the response converges to the reference level. This increase in overshoot accompanies the reduction in settling time achieved with this controller structure, illustrating the trade-off between response speed and transient overshoot. Its acceptability depends on the specific requirements of the application. When stricter overshoot constraints are imposed, reference conditioning (for example through a prefilter) may be considered without altering the general PI/PID selection principle proposed in this work.

### 5.2. Sensitivity Analysis of Tuning Parameters

This section analyzes the influence of the tuning parameters $\lambda$, $\zeta^{\mathrm{PI}}$, and $\zeta^{\mathrm{PID}}$ on the energy costs, time-domain performance, and Nash equilibrium structure while keeping the remaining parameters at their nominal values. The nominal tuning configuration has already been analyzed in Section 5.1.

#### 5.2.1. Sensitivity to the Common Exponential Decay Rate $\lambda$

The common exponential decay rate is varied over $\lambda \in \{0.27, 0.40, 1.65, 2.00\}$ while the remaining parameters are kept at their nominal values. For each value of $\lambda$, the four strategy profiles are evaluated using Algorithm 1 to analyze the costs $J_i$, $i \in \{1, 2\}$, time-domain performance, and Nash equilibrium. The corresponding results are summarized in Table 2.

**Table 2.** Influence of $\lambda$ on the costs, time-domain performance, and Nash equilibrium.

| $\lambda$ | $s = (s_1, s_2)$ | $\mathcal{P}_1$ | | | | $\mathcal{P}_2$ | | | | Nash Equilibrium |
|---|---|---|---|---|---|---|---|---|---|---|
| | | $J_1$ | $M_{p,1}$ (%) | $T_{s,1}$ (s) | $e_{ss,1}$ | $J_2$ | $M_{p,2}$ (%) | $T_{s,2}$ (s) | $e_{ss,2}$ | |
| 0.27 | (PI, PI) | 144.4925 | 13.5372 | 19.460 | $1.79 \times 10^{-2}$ | 144.4925 | 13.5372 | 19.460 | $1.79 \times 10^{-2}$ | (PI, PI) |
| | (PI, PID) | 145.0110 | 13.5372 | 19.460 | $1.79 \times 10^{-2}$ | 145.2024 | 20.7968 | 12.679 | $5.72 \times 10^{-3}$ | |
| | (PID, PI) | 145.2024 | 20.7968 | 12.679 | $5.72 \times 10^{-3}$ | 145.0110 | 13.5372 | 19.460 | $1.79 \times 10^{-2}$ | |
| | (PID, PID) | 145.0773 | 20.7968 | 12.679 | $5.72 \times 10^{-3}$ | 145.0773 | 20.7968 | 12.679 | $5.72 \times 10^{-3}$ | |
| 0.40 | (PI, PI) | 145.0707 | 13.5389 | 13.135 | $2.11 \times 10^{-3}$ | 145.0707 | 13.5389 | 13.135 | $2.11 \times 10^{-3}$ | (PID, PID) |
| | (PI, PID) | 146.7254 | 13.5389 | 13.135 | $2.11 \times 10^{-3}$ | 143.9879 | 20.8010 | 8.558 | $3.43 \times 10^{-4}$ | |
| | (PID, PI) | 143.9879 | 20.8010 | 8.558 | $3.43 \times 10^{-4}$ | 146.7254 | 13.5389 | 13.135 | $2.11 \times 10^{-3}$ | |
| | (PID, PID) | 145.1795 | 20.8010 | 8.558 | $3.43 \times 10^{-4}$ | 145.1795 | 20.8010 | 8.558 | $3.43 \times 10^{-4}$ | |
| 1.65 | (PI, PI) | 146.3612 | 13.5559 | 3.183 | $1.41 \times 10^{-13}$ | 146.3612 | 13.5559 | 3.183 | $1.41 \times 10^{-13}$ | (PI, PI) (PID, PID) |
| | (PI, PID) | 146.7657 | 13.5559 | 3.183 | $1.41 \times 10^{-13}$ | 146.4039 | 20.8419 | 2.073 | $4.33 \times 10^{-15}$ | |
| | (PID, PI) | 146.4039 | 20.8419 | 2.073 | $4.33 \times 10^{-15}$ | 146.7657 | 13.5559 | 3.183 | $1.41 \times 10^{-13}$ | |
| | (PID, PID) | 146.6956 | 20.8419 | 2.073 | $4.22 \times 10^{-15}$ | 146.6956 | 20.8419 | 2.073 | $4.22 \times 10^{-15}$ | |
| 2.00 | (PI, PI) | 146.7133 | 13.5606 | 2.626 | $<10^{-14}$ | 146.7133 | 13.5606 | 2.626 | $<10^{-14}$ | (PI, PI) |
| | (PI, PID) | 147.0149 | 13.5606 | 2.626 | $<10^{-14}$ | 146.9104 | 20.8534 | 1.710 | $<10^{-14}$ | |
| | (PID, PI) | 146.9104 | 20.8534 | 1.710 | $<10^{-14}$ | 147.0149 | 13.5606 | 2.626 | $<10^{-14}$ | |
| | (PID, PID) | 147.1189 | 20.8534 | 1.710 | $<10^{-14}$ | 147.1189 | 20.8534 | 1.710 | $<10^{-14}$ | |

Table 2 shows that increasing $\lambda$ significantly accelerates the closed-loop dynamics: the settling times decrease and the residual errors at the end of the simulation horizon rapidly become negligible, while the overshoots remain almost unchanged. This behavior follows directly from the pole-placement procedure: $\lambda$ determines the real part of the poles and scales their natural frequency. Since the damping ratios are kept fixed, the response is essentially compressed in time without a significant change in its shape. At the same time, the proportional and integral gains increase with $\lambda$ according to Equations (26) and (32), resulting in auxiliary control actions $v_i(t)$ that are more intense but shorter in duration. In the physical control inputs given by Equation (20), this effect combines with the compensation terms associated with leakage and hydraulic coupling. The cost $J_i$, defined by Equation (34), results from a trade-off between the magnitude and duration of the control effort, which differs between the PI and PID structures. Consequently, their relative energy advantages may reverse as $\lambda$ varies. For $\lambda = 0.27$, these cost differences make PI the best response for both players, leading to $(\mathrm{PI}, \mathrm{PI})$. For $\lambda = 0.40$, as in the nominal case $\lambda = 1$, $(\mathrm{PID}, \mathrm{PID})$ is the unique equilibrium. At $\lambda = 1.65$, each controller structure is a best response to itself, leading to the coexistence of $(\mathrm{PI}, \mathrm{PI})$ and $(\mathrm{PID}, \mathrm{PID})$. Finally, for $\lambda = 2$, $(\mathrm{PI}, \mathrm{PI})$ again becomes the unique equilibrium. These Nash equilibrium

transitions correspond to reversals of the best responses induced by the redistribution of control effort between the two controller structures.

#### 5.2.2. Sensitivity to the PI Damping Ratio $\zeta^{\mathrm{PI}}$

The PI damping ratio is varied over $\zeta^{\mathrm{PI}} \in \{0.60, 0.80, 0.90, 0.95\}$ while the remaining parameters are kept at their nominal values. For each value of $\zeta^{\mathrm{PI}}$, the four strategy profiles are evaluated to analyze the costs $J_i$, $i \in \{1, 2\}$, time-domain performance, and Nash equilibrium. The corresponding results are presented in Table 3.

**Table 3.** Influence of $\zeta^{\mathrm{PI}}$ on the costs, time-domain performance, and Nash equilibrium.

| $\zeta^{\mathrm{PI}}$ | $s = (s_1, s_2)$ | $\mathcal{P}_1$ | | | | $\mathcal{P}_2$ | | | | Nash Equilibrium |
|---|---|---|---|---|---|---|---|---|---|---|
| | | $J_1$ | $M_{p,1}$ (%) | $T_{s,1}$ (s) | $e_{ss,1}$ | $J_2$ | $M_{p,2}$ (%) | $T_{s,2}$ (s) | $e_{ss,2}$ | |
| 0.60 | (PI, PI) | 146.0668 | 24.9322 | 3.974 | $1.38 \times 10^{-9}$ | 146.0668 | 24.9322 | 3.974 | $1.38 \times 10^{-9}$ | (PID, PID) |
| | (PI, PID) | 146.2904 | 24.9322 | 3.974 | $1.38 \times 10^{-9}$ | 145.7825 | 20.8207 | 3.422 | $9.85 \times 10^{-10}$ | |
| | (PID, PI) | 145.7825 | 20.8207 | 3.422 | $9.85 \times 10^{-10}$ | 146.2904 | 24.9322 | 3.974 | $1.38 \times 10^{-9}$ | |
| | (PID, PID) | 145.9092 | 20.8207 | 3.422 | $9.85 \times 10^{-10}$ | 145.9092 | 20.8207 | 3.422 | $9.85 \times 10^{-10}$ | |
| 0.80 | (PI, PI) | 145.8206 | 18.0025 | 3.981 | $2.99 \times 10^{-9}$ | 145.8206 | 18.0025 | 3.981 | $2.99 \times 10^{-9}$ | (PI, PI) |
| | (PI, PID) | 145.8340 | 18.0025 | 3.981 | $2.99 \times 10^{-9}$ | 145.9577 | 20.8207 | 3.422 | $9.85 \times 10^{-10}$ | |
| | (PID, PI) | 145.9577 | 20.8207 | 3.422 | $9.85 \times 10^{-10}$ | 145.8340 | 18.0025 | 3.981 | $2.99 \times 10^{-9}$ | |
| | (PID, PID) | 145.9092 | 20.8207 | 3.422 | $9.85 \times 10^{-10}$ | 145.9092 | 20.8207 | 3.422 | $9.85 \times 10^{-10}$ | |
| 0.90 | (PI, PI) | 145.7542 | 15.5461 | 4.613 | $7.55 \times 10^{-10}$ | 145.7542 | 15.5461 | 4.613 | $7.55 \times 10^{-10}$ | (PI, PI) (PID, PID) |
| | (PI, PID) | 145.9681 | 15.5461 | 4.613 | $7.55 \times 10^{-10}$ | 145.8224 | 20.8207 | 3.422 | $9.85 \times 10^{-10}$ | |
| | (PID, PI) | 145.8224 | 20.8207 | 3.422 | $9.85 \times 10^{-10}$ | 145.9681 | 15.5461 | 4.613 | $7.55 \times 10^{-10}$ | |
| | (PID, PID) | 145.9092 | 20.8207 | 3.422 | $9.85 \times 10^{-10}$ | 145.9092 | 20.8207 | 3.422 | $9.85 \times 10^{-10}$ | |
| 0.95 | (PI, PI) | 145.7286 | 14.4968 | 4.933 | $1.21 \times 10^{-10}$ | 145.7286 | 14.4968 | 4.933 | $1.21 \times 10^{-10}$ | (PID, PID) |
| | (PI, PID) | 146.2353 | 14.4968 | 4.933 | $1.21 \times 10^{-10}$ | 145.5597 | 20.8207 | 3.422 | $9.85 \times 10^{-10}$ | |
| | (PID, PI) | 145.5597 | 20.8207 | 3.422 | $9.85 \times 10^{-10}$ | 146.2353 | 14.4968 | 4.933 | $1.21 \times 10^{-10}$ | |
| | (PID, PID) | 145.9092 | 20.8207 | 3.422 | $9.85 \times 10^{-10}$ | 145.9092 | 20.8207 | 3.422 | $9.85 \times 10^{-10}$ | |

Table 3 shows that $\zeta^{\mathrm{PI}}$ mainly affects the shape of the PI-controlled response. For a fixed $\lambda$, the real part of the PI poles remains equal to $-\lambda$, while their imaginary part decreases as $\zeta^{\mathrm{PI}}$ increases. Consequently, the PI overshoot decreases from 24.93% for $\zeta^{\mathrm{PI}} = 0.60$ to 14.50% for $\zeta^{\mathrm{PI}} = 0.95$ at the cost of a longer settling time. The PID performance remains unchanged because its tuning is kept constant. According to Equation (26), $K_P^{\mathrm{PI}}$ remains constant, whereas $K_I^{\mathrm{PI}}$ decreases as $\zeta^{\mathrm{PI}}$ increases. The resulting modification of the PI trajectory then affects the physical control inputs and the interconnection flow in the mixed profiles, thereby modifying the costs $J_i$ and potentially reversing the best responses. Thus, (PID, PID) is the unique equilibrium for $\zeta^{\mathrm{PI}} = 0.60$, while (PI, PI) becomes the unique equilibrium for $\zeta^{\mathrm{PI}} = 0.80$. The two symmetric equilibria coexist for $\zeta^{\mathrm{PI}} = 0.90$, whereas (PID, PID) again becomes the unique equilibrium for $\zeta^{\mathrm{PI}} = 0.95$ and for the nominal value $\zeta^{\mathrm{PI}} = 1$. These changes show that the PI damping ratio affects not only the transient performance but also the energetic interaction between the two loops, which is responsible for the observed Nash equilibrium transitions.

#### 5.2.3. Sensitivity to the PID Damping Ratio $\zeta^{\mathrm{PID}}$

The PID damping ratio is varied over $\zeta^{\mathrm{PID}} \in \{0.30, 0.35, 0.50, 0.90\}$ while the remaining parameters are kept at their nominal values. For each value of $\zeta^{\mathrm{PID}}$, the four strategy profiles are evaluated to analyze the costs $J_i$, $i \in \{1, 2\}$, time-domain performance, and Nash equilibrium. The corresponding results are presented in Table 4.

**Table 4.** Influence of $\zeta^{\mathrm{PID}}$ on the costs, time-domain performance, and Nash equilibrium.

| $\zeta^{\mathrm{PID}}$ | $s=(s_1,s_2)$ | $\mathcal{P}_1$ | | | | $\mathcal{P}_2$ | | | | Nash Equilibrium |
|---|---|---|---|---|---|---|---|---|---|---|
| | | $J_1$ | $M_{p,1}$ (%) | $T_{s,1}$ (s) | $e_{ss,1}$ | $J_2$ | $M_{p,2}$ (%) | $T_{s,2}$ (s) | $e_{ss,2}$ | |
| 0.30 | (PI, PI) | 145.7067 | 13.5471 | 5.253 | $3.49\times10^{-8}$ | 145.7067 | 13.5471 | 5.253 | $3.49\times10^{-8}$ | (PI, PI) |
| | (PI, PID) | 147.5914 | 13.5471 | 5.253 | $3.49\times10^{-8}$ | 146.6206 | 45.2976 | 3.870 | $9.05\times10^{-10}$ | |
| | (PID, PI) | 146.6206 | 45.2976 | 3.870 | $9.05\times10^{-10}$ | 147.5914 | 13.5471 | 5.253 | $3.49\times10^{-8}$ | |
| | (PID, PID) | 147.7636 | 45.2976 | 3.870 | $9.05\times10^{-10}$ | 147.7636 | 45.2976 | 3.870 | $9.05\times10^{-10}$ | |
| 0.35 | (PI, PI) | 145.7067 | 13.5471 | 5.253 | $3.49\times10^{-8}$ | 145.7067 | 13.5471 | 5.253 | $3.49\times10^{-8}$ | (PI, PI) (PID, PID) |
| | (PI, PID) | 147.3905 | 13.5471 | 5.253 | $3.49\times10^{-8}$ | 146.1429 | 40.5393 | 3.637 | $1.81\times10^{-9}$ | |
| | (PID, PI) | 146.1429 | 40.5393 | 3.637 | $1.81\times10^{-9}$ | 147.3905 | 13.5471 | 5.253 | $3.49\times10^{-8}$ | |
| | (PID, PID) | 147.1617 | 40.5393 | 3.637 | $1.81\times10^{-9}$ | 147.1617 | 40.5393 | 3.637 | $1.81\times10^{-9}$ | |
| 0.50 | (PI, PI) | 145.7067 | 13.5471 | 5.253 | $3.49\times10^{-8}$ | 145.7067 | 13.5471 | 5.253 | $3.49\times10^{-8}$ | (PID, PID) |
| | (PI, PID) | 146.9076 | 13.5471 | 5.253 | $3.49\times10^{-8}$ | 145.5460 | 29.9159 | 3.710 | $1.75\times10^{-9}$ | |
| | (PID, PI) | 145.5460 | 29.9159 | 3.710 | $1.75\times10^{-9}$ | 146.9076 | 13.5471 | 5.253 | $3.49\times10^{-8}$ | |
| | (PID, PID) | 146.3148 | 29.9159 | 3.710 | $1.75\times10^{-9}$ | 146.3148 | 29.9159 | 3.710 | $1.75\times10^{-9}$ | |
| 0.90 | (PI, PI) | 145.7067 | 13.5471 | 5.253 | $3.49\times10^{-8}$ | 145.7067 | 13.5471 | 5.253 | $3.49\times10^{-8}$ | (PID, PID) |
| | (PI, PID) | 146.1932 | 13.5471 | 5.253 | $3.49\times10^{-8}$ | 145.3128 | 15.5461 | 4.613 | $7.55\times10^{-10}$ | |
| | (PID, PI) | 145.3128 | 15.5461 | 4.613 | $7.55\times10^{-10}$ | 146.1932 | 13.5471 | 5.253 | $3.49\times10^{-8}$ | |
| | (PID, PID) | 145.7542 | 15.5461 | 4.613 | $7.55\times10^{-10}$ | 145.7542 | 15.5461 | 4.613 | $7.55\times10^{-10}$ | |

Table 4 shows that increasing $\zeta^{\mathrm{PID}}$ mainly improves the damping of the PID-controlled response. For fixed $\lambda$, increasing $\zeta^{\mathrm{PID}}$ reduces the imaginary part of the PID poles and significantly decreases the overshoot, from 45.30% for $\zeta^{\mathrm{PID}}=0.30$ to 15.55% for $\zeta^{\mathrm{PID}}=0.90$. The PI performance remains unchanged because its tuning is kept constant. The variation of $\zeta^{\mathrm{PID}}$ also modifies the gains given by Equation (32), and consequently the auxiliary control actions $v_i(t)$ defined by Equation (27). These changes affect the physical control inputs and the costs $J_i$, particularly in the mixed profiles where the hydraulic coupling is active. For $\zeta^{\mathrm{PID}}=0.30$, the costs associated with the PID structure are sufficiently high to make $(\mathrm{PI},\mathrm{PI})$ the unique equilibrium. At $\zeta^{\mathrm{PID}}=0.35$, the best responses lead to the coexistence of $(\mathrm{PI},\mathrm{PI})$ and $(\mathrm{PID},\mathrm{PID})$. For $\zeta^{\mathrm{PID}}=0.50$ and 0.90, the PID structure becomes energetically more favorable under unilateral deviations and $(\mathrm{PID},\mathrm{PID})$ becomes the unique equilibrium, as in the nominal configuration. Thus, $\zeta^{\mathrm{PID}}$ affects both the transient behavior of the PID controller and the relative costs that determine the best responses and the structure of the Nash equilibrium.

### *5.3. Sensitivity Analysis of Physical Parameters and Operating Conditions*

This section investigates the influence of the leakage parameters, hydraulic coupling parameter, and initial conditions on the energy costs and the structure of the Nash equilibrium. In each analysis, only the parameter or operating condition under study is varied, while the remaining parameters are kept at their nominal values defined in Section 5.1.

#### 5.3.1. Sensitivity to the Leakage Parameters $b_1$ and $b_2$

The leakage parameter $b_2$ is varied over $b_2 \in \{0.20, 0.80\}$ while $b_1 = 0.60$ and the remaining parameters are kept at their nominal values. For each value of $b_2$, the four strategy profiles are evaluated to analyze the costs $J_i$, $i \in \{1,2\}$, time-domain performance, and Nash equilibrium. Owing to the symmetry of the nominal configuration, the same analysis applies when varying $b_1$ instead of $b_2$, up to an interchange of the two players. The corresponding results are presented in Table 5.

**Table 5.** Influence of the leakage parameter $b_2$ on the costs, time-domain performance, and Nash equilibrium.

| $b_2$ | $s = (s_1, s_2)$ | $\mathcal{P}_1$ | | | | $\mathcal{P}_2$ | | | | Nash Equilibrium |
|---|---|---|---|---|---|---|---|---|---|---|
| | | $J_1$ | $M_{p,1}$ (%) | $T_{s,1}$ (s) | $e_{ss,1}$ | $J_2$ | $M_{p,2}$ (%) | $T_{s,2}$ (s) | $e_{ss,2}$ | |
| 0.20 | (PI, PI) | 145.7067 | 13.5471 | 5.253 | $3.49 \times 10^{-8}$ | 17.8507 | 13.5471 | 5.253 | $3.49 \times 10^{-8}$ | (PID, PI) |
| | (PI, PID) | 146.4926 | 13.5471 | 5.253 | $3.49 \times 10^{-8}$ | 18.0127 | 20.8207 | 3.422 | $9.85 \times 10^{-10}$ | |
| | (PID, PI) | 145.3095 | 20.8207 | 3.422 | $9.85 \times 10^{-10}$ | 18.0272 | 13.5471 | 5.253 | $3.49 \times 10^{-8}$ | |
| | (PID, PID) | 145.9092 | 20.8207 | 3.422 | $9.85 \times 10^{-10}$ | 18.0534 | 20.8207 | 3.422 | $9.85 \times 10^{-10}$ | |
| 0.80 | (PI, PI) | 145.7067 | 13.5471 | 5.253 | $3.49 \times 10^{-8}$ | 256.7238 | 13.5471 | 5.253 | $3.49 \times 10^{-8}$ | (PID, PID) |
| | (PI, PID) | 146.4926 | 13.5471 | 5.253 | $3.49 \times 10^{-8}$ | 256.0469 | 20.8207 | 3.422 | $9.85 \times 10^{-10}$ | |
| | (PID, PI) | 145.3095 | 20.8207 | 3.422 | $9.85 \times 10^{-10}$ | 257.8144 | 13.5471 | 5.253 | $3.49 \times 10^{-8}$ | |
| | (PID, PID) | 145.9092 | 20.8207 | 3.422 | $9.85 \times 10^{-10}$ | 256.9261 | 20.8207 | 3.422 | $9.85 \times 10^{-10}$ | |

Table 5 shows that varying $b_2$ can modify the structure of the Nash equilibrium. Since $b_2$ does not enter the controller tuning laws, it does not affect the PI/PID gains or the auxiliary control actions $v_i(t)$. As long as the non-negativity constraint remains inactive, the auxiliary dynamics are unchanged; consequently, for a given controller structure, the overshoot, settling time, and residual error remain unchanged. In contrast, $b_2$ appears directly in the physical control input $u_2(t)$ through the leakage compensation term $b_2\sqrt{2g\,y_2(t)}$. Its variation modifies the control effort and the energy cost $J_2$, which can change the best response of player $\mathcal{P}_2$. Thus, for $b_2 = 0.20$, the unique equilibrium becomes (PID, PI), whereas for $b_2 = 0.80$ the equilibrium is (PID, PID), identical to that of the reference configuration studied in Section 5.1.

#### 5.3.2. Sensitivity to the Hydraulic Coupling Parameter $a$

The hydraulic coupling parameter is varied over $a \in \{0.02, 0.03, 0.20\}$ while the remaining parameters are kept at their nominal values. For each value of $a$, the four strategy profiles are evaluated to analyze the costs $J_i$, $i \in \{1, 2\}$, time-domain performance, and Nash equilibrium. The corresponding results are presented in Table 6.

**Table 6.** Influence of the hydraulic coupling parameter $a$ on the costs, time-domain performance, and Nash equilibrium.

| $a$ | $s = (s_1, s_2)$ | $\mathcal{P}_1$ | | | | $\mathcal{P}_2$ | | | | Nash Equilibrium |
|---|---|---|---|---|---|---|---|---|---|---|
| | | $J_1$ | $M_{p,1}$ (%) | $T_{s,1}$ (s) | $e_{ss,1}$ | $J_2$ | $M_{p,2}$ (%) | $T_{s,2}$ (s) | $e_{ss,2}$ | |
| 0.02 | (PI, PI) | 145.7067 | 13.5471 | 5.253 | $3.49 \times 10^{-8}$ | 145.7067 | 13.5471 | 5.253 | $3.49 \times 10^{-8}$ | (PI, PI) |
| | (PI, PID) | 145.8550 | 13.5471 | 5.253 | $3.49 \times 10^{-8}$ | 145.7804 | 20.8207 | 3.422 | $9.85 \times 10^{-10}$ | |
| | (PID, PI) | 145.7804 | 20.8207 | 3.422 | $9.85 \times 10^{-10}$ | 145.8550 | 13.5471 | 5.253 | $3.49 \times 10^{-8}$ | |
| | (PID, PID) | 145.9092 | 20.8207 | 3.422 | $9.85 \times 10^{-10}$ | 145.9092 | 20.8207 | 3.422 | $9.85 \times 10^{-10}$ | |
| 0.03 | (PI, PI) | 145.7067 | 13.5471 | 5.253 | $3.49 \times 10^{-8}$ | 145.7067 | 13.5471 | 5.253 | $3.49 \times 10^{-8}$ | (PI, PI) (PID, PID) |
| | (PI, PID) | 145.9309 | 13.5471 | 5.253 | $3.49 \times 10^{-8}$ | 145.7177 | 20.8207 | 3.422 | $9.85 \times 10^{-10}$ | |
| | (PID, PI) | 145.7177 | 20.8207 | 3.422 | $9.85 \times 10^{-10}$ | 145.9309 | 13.5471 | 5.253 | $3.49 \times 10^{-8}$ | |
| | (PID, PID) | 145.9092 | 20.8207 | 3.422 | $9.85 \times 10^{-10}$ | 145.9092 | 20.8207 | 3.422 | $9.85 \times 10^{-10}$ | |
| 0.20 | (PI, PI) | 145.7067 | 13.5471 | 5.253 | $3.49 \times 10^{-8}$ | 145.7067 | 13.5471 | 5.253 | $3.49 \times 10^{-8}$ | (PID, PID) |
| | (PI, PID) | 147.3891 | 13.5471 | 5.253 | $3.49 \times 10^{-8}$ | 144.8204 | 20.8207 | 3.422 | $9.85 \times 10^{-10}$ | |
| | (PID, PI) | 144.8204 | 20.8207 | 3.422 | $9.85 \times 10^{-10}$ | 147.3891 | 13.5471 | 5.253 | $3.49 \times 10^{-8}$ | |
| | (PID, PID) | 145.9092 | 20.8207 | 3.422 | $9.85 \times 10^{-10}$ | 145.9092 | 20.8207 | 3.422 | $9.85 \times 10^{-10}$ | |

Table 6 shows that varying $a$ can modify the structure of the Nash equilibrium. The parameter $a$ does not enter the controller tuning laws, and as such does not affect the PI/PID gains or the auxiliary control actions $v_i(t)$. As long as the non-negativity constraint

on the control inputs remains inactive, the auxiliary dynamics are still given by $\dot{y}_i = v_i$. Consequently, for a given controller structure, the overshoot, settling time, and residual error remain unchanged when $a$ varies. In contrast, $a$ directly scales the interconnection flow $Q_{12}$, which enters the physical control inputs $u_1(t)$ and $u_2(t)$ with opposite signs in Equation (20). For symmetric strategy profiles, $y_1(t) = y_2(t)$, so that $Q_{12}(t) = 0$, and their costs remain unchanged. For asymmetric PI/PID profiles, however, the two level trajectories differ and $Q_{12}(t) \neq 0$. Varying $a$ modifies the corresponding control efforts and energy costs, which changes the best-response structure of the game. Thus, for $a = 0.02$, the unique equilibrium is (PI, PI); for $a = 0.03$, both (PI, PI) and (PID, PID) are Nash equilibria; and for $a = 0.20$, the unique equilibrium is (PID, PID), identical to that obtained for the reference configuration studied in Section 5.1.

#### 5.3.3. Sensitivity to the Initial Conditions

The initial condition of the second tank is varied over $y_2(0) \in \{0.30, 1.00\}$ while $y_1(0) = 0.10$ and the remaining parameters are kept at their nominal values. For each value of $y_2(0)$, the four strategy profiles are evaluated to analyze the costs $J_i$, $i \in \{1, 2\}$, time-domain performance, and Nash equilibrium. Owing to the symmetry of the nominal configuration, the same analysis applies when varying $y_1(0)$ instead of $y_2(0)$, up to an interchange of the two players. The corresponding results are presented in Table 7.

**Table 7.** Influence of the initial condition $y_2(0)$ on the costs, time-domain performance, and Nash equilibrium.

| $y_2(0)$ | $s = (s_1, s_2)$ | $\mathcal{P}_1$ | | | | $\mathcal{P}_2$ | | | | Nash Equilibrium |
|---|---|---|---|---|---|---|---|---|---|---|
| | | $J_1$ | $M_{p,1}$ (%) | $T_{s,1}$ (s) | $e_{ss,1}$ | $J_2$ | $M_{p,2}$ (%) | $T_{s,2}$ (s) | $e_{ss,2}$ | |
| 0.30 | (PI, PI) | 146.7308 | 13.5471 | 5.253 | $3.49 \times 10^{-8}$ | 143.8731 | 13.5471 | 4.921 | $2.72 \times 10^{-8}$ | (PID, PID) |
| | (PI, PID) | 146.6936 | 13.5471 | 5.253 | $3.49 \times 10^{-8}$ | 144.1536 | 20.8207 | 3.327 | $7.66 \times 10^{-10}$ | |
| | (PID, PI) | 145.2238 | 20.8207 | 3.422 | $9.85 \times 10^{-10}$ | 145.6910 | 13.5471 | 4.921 | $2.72 \times 10^{-8}$ | |
| | (PID, PID) | 146.2406 | 20.8207 | 3.422 | $9.85 \times 10^{-10}$ | 144.6816 | 20.8207 | 3.327 | $7.66 \times 10^{-10}$ | |
| 1.00 | (PI, PI) | 147.9477 | 13.5471 | 5.253 | $3.49 \times 10^{-8}$ | 139.2273 | 0 | 0 | 0 | (PID, PI) (PID, PID) |
| | (PI, PID) | 147.9477 | 13.5471 | 5.253 | $3.49 \times 10^{-8}$ | 139.2273 | 0 | 0 | 0 | |
| | (PID, PI) | 146.6752 | 20.8207 | 3.422 | $9.85 \times 10^{-10}$ | 140.6699 | 0 | 0 | 0 | |
| | (PID, PID) | 146.6752 | 20.8207 | 3.422 | $9.85 \times 10^{-10}$ | 140.6699 | 0 | 0 | 0 | |

Table 7 shows that varying $y_2(0)$ can modify the structure of the Nash equilibrium. The initial condition does not affect the PI/PID controller gains; however, it directly modifies the initial tracking error $e_2(0) = y_{2,\text{ref}} - y_2(0)$, and consequently both the auxiliary control action $v_2(t)$ and the amplitude of the transient response of the second tank. As $y_2(0)$ approaches the reference, the initial error decreases. For a given controller structure, the dynamic shape of the response is preserved, which explains why the relative overshoot remains unchanged while the settling time and residual error decrease. Thus, for $y_2(0) = 0.30$, the settling times of the second tank become 4.921 s with PI and 3.327 s with PID, compared with 5.253 s and 3.422 s, respectively, in the reference configuration $y_1(0) = y_2(0) = 0.10$ studied in Section 5.1. For $y_2(0) = 1.00$, the second tank starts exactly at its reference; consequently, under the decoupled auxiliary dynamics, $e_2(t) = 0$ and $v_2(t) = 0$ throughout the simulation horizon, and no transient response occurs for this tank. The PI and PID strategies of player $\mathcal{P}_2$ become equivalent in terms of the closed-loop response of tank $R_2$. This variation in $y_2(0)$ also affects the physical control inputs and the energy costs, leading to the two Nash equilibria (PID, PI) and (PID, PID), whereas for $y_2(0) = 0.30$ the unique equilibrium remains (PID, PID).

### *5.4. Robustness Analysis Under Parametric Model Uncertainties*

The analyses conducted in Sections 5.2 and 5.3 assume exact knowledge of the hydraulic parameters used in the compensation law. Here, we assess the robustness of the proposed framework when the actual plant parameters differ from the values used by the controller. Two representative parameters are considered. The parameter $a$ is selected because it directly enters the interconnection flow $Q_{12}$, allowing the effect of uncertainty in the hydraulic coupling between the two tanks to be evaluated. The parameter $b_1$ is selected to represent a local uncertainty in the outlet flow of one tank. A separate analysis of $b_2$ is not required because the two tanks are symmetric under the nominal configuration of Section 5.1; therefore, the effects of uncertainty in $b_2$ can be inferred from those obtained for $b_1$ by interchanging the indices 1 and 2. All other system parameters are kept at the nominal values of the same configuration.

Robustness is then assessed by distinguishing the parameters used in the compensation law from those that actually govern the plant dynamics. The controller retains the nominal values $\hat{a} = 0.10$ and $\hat{b}_1 = 0.60$, whereas the plant evolves with the actual values $a$ and $b_1$, which may deviate from these nominal values.

By substituting the compensation law of Equation (20), evaluated using $\hat{a}$ and $\hat{b}_1$, into the actual plant dynamics, the closed-loop dynamics become

$$\begin{cases} A\dot{y}_1(t) = Av_1(t) + (\hat{b}_1 - b_1)\sqrt{2g\,y_1(t)} + (\hat{a} - a)\ \mathrm{sign}\big(y_1(t) - y_2(t)\big)\sqrt{2g\,|y_1(t) - y_2(t)|}, \\ A\dot{y}_2(t) = Av_2(t) - (\hat{a} - a)\ \mathrm{sign}\big(y_1(t) - y_2(t)\big)\sqrt{2g\,|y_1(t) - y_2(t)|}. \end{cases} \tag{40}$$

Equation (40) highlights the residual terms induced by model uncertainties. The mismatch $\hat{a} - a$ affects the hydraulic coupling between the two tanks, whereas the mismatch $\hat{b}_1 - b_1$ acts directly on the dynamics of the first tank. When $a = \hat{a}$ and $b_1 = \hat{b}_1$, these residual terms vanish and the nominal dynamics $\dot{y}_i = v_i$ are recovered.

For each uncertainty scenario, the general procedure of Algorithm 1 is retained. The same strategy profiles, PI/PID control laws, and tuning parameters are used. The physical control inputs are computed according to the structure of Equation (20) from the measured liquid levels $y_1(t)$ and $y_2(t)$, while the compensation law retains the nominal values $\hat{a}$ and $\hat{b}_1$, with all other parameters kept at their nominal values. At each simulation step, the level derivatives $\dot{y}_1(t)$ and $\dot{y}_2(t)$ are then computed from Equation (40) using the perturbed actual value of either $a$ or $b_1$, after which the levels are updated numerically; hence, the considered parameter variations are neither known nor compensated for by the controller. The energy costs, performance indices, and Nash equilibria are then determined following the same steps as those defined in Algorithm 1.

We first consider a $\pm 10\%$ uncertainty in the hydraulic coupling parameter, with $a \in \{0.09, 0.11\}$, while the controller retains the nominal value $\hat{a} = 0.10$. The corresponding results are reported in Table 8.

Table 8 shows that uncertainty in $a$ mainly affects the asymmetric profiles $(\mathrm{PI}, \mathrm{PID})$ and $(\mathrm{PID}, \mathrm{PI})$. According to Equation (40), the mismatch $\hat{a} - a$ directly multiplies the coupling term that depends on $y_1 - y_2$. For the symmetric profiles, the two liquid levels evolve identically, so that $y_1 - y_2 = 0$ and this residual term vanishes; in contrast, the mixed profiles generate different transient responses in the two tanks, thereby activating the hydraulic coupling. The change in sign of $\hat{a} - a$ on either side of the nominal value changes the direction of the residual coupling term, the level trajectories, and consequently the control effort associated with each strategy.

**Table 8.** Influence of uncertainty in the hydraulic coupling parameter $a$ on the costs, time-domain performance, and Nash equilibrium.

| $a$ | $\hat{a}$ | $s = (s_1, s_2)$ | $\mathcal{P}_1$ | | | | $\mathcal{P}_2$ | | | | Nash Equilibrium |
|---|---|---|---|---|---|---|---|---|---|---|---|
| | | | $J_1$ | $M_{p,1}$ (%) | $T_{s,1}$ (s) | $e_{ss,1}$ | $J_2$ | $M_{p,2}$ (%) | $T_{s,2}$ (s) | $e_{ss,2}$ | |
| 0.09 | 0.10 | (PI, PI) | 145.7067 | 13.5471 | 5.253 | $3.49 \times 10^{-8}$ | 145.7067 | 13.5471 | 5.253 | $3.49 \times 10^{-8}$ | (PI, PI) |
| | | (PI, PID) | 145.9080 | 13.1608 | 5.397 | $8.20 \times 10^{-4}$ | 145.9000 | 21.2408 | 3.307 | $4.34 \times 10^{-4}$ | |
| | | (PID, PI) | 145.9000 | 21.2408 | 3.307 | $4.34 \times 10^{-4}$ | 145.9080 | 13.1608 | 5.397 | $8.20 \times 10^{-4}$ | |
| | | (PID, PID) | 145.9092 | 20.8207 | 3.422 | $9.85 \times 10^{-10}$ | 145.9092 | 20.8207 | 3.422 | $9.85 \times 10^{-10}$ | |
| 0.11 | 0.10 | (PI, PI) | 145.7067 | 13.5471 | 5.253 | $3.49 \times 10^{-8}$ | 145.7067 | 13.5471 | 5.253 | $3.49 \times 10^{-8}$ | (PID, PID) |
| | | (PI, PID) | 146.9830 | 13.9081 | 5.070 | $5.39 \times 10^{-5}$ | 144.8200 | 20.4435 | 3.530 | $2.11 \times 10^{-5}$ | |
| | | (PID, PI) | 144.8200 | 20.4435 | 3.530 | $2.11 \times 10^{-5}$ | 146.9830 | 13.9081 | 5.070 | $5.39 \times 10^{-5}$ | |
| | | (PID, PID) | 145.9092 | 20.8207 | 3.422 | $9.85 \times 10^{-10}$ | 145.9092 | 20.8207 | 3.422 | $9.85 \times 10^{-10}$ | |

This mechanism directly modifies the players' best responses. For $a = 0.09$, PI is the best response of the first player both against PI $(145.7067 < 145.9000)$ and against PID $(145.9080 < 145.9092)$. By symmetry, the same preference is obtained for the second player, and the equilibrium shifts to $(\mathrm{PI}, \mathrm{PI})$. Conversely, for $a = 0.11$, PID becomes the best response of both players, thereby restoring the nominal equilibrium $(\mathrm{PID}, \mathrm{PID})$. Hence, the change in equilibrium results from a reversal in the energy-based ranking of the strategies induced by imperfect compensation of the hydraulic coupling rather than from a loss of level convergence, since the steady-state errors remain small in all cases.

We now consider a $\pm 10\%$ uncertainty in the outlet parameter of the first tank, with $b_1 \in \{0.54, 0.66\}$ and $\hat{b}_1 = 0.60$. The corresponding results are reported in Table 9.

**Table 9.** Influence of uncertainty in the outlet parameter $b_1$ on the costs, time-domain performance, and Nash equilibrium.

| $b_1$ | $\hat{b}_1$ | $s = (s_1, s_2)$ | $\mathcal{P}_1$ | | | | $\mathcal{P}_2$ | | | | Nash Equilibrium |
|---|---|---|---|---|---|---|---|---|---|---|---|
| | | | $J_1$ | $M_{p,1}$ (%) | $T_{s,1}$ (s) | $e_{ss,1}$ | $J_2$ | $M_{p,2}$ (%) | $T_{s,2}$ (s) | $e_{ss,2}$ | |
| 0.54 | 0.60 | (PI, PI) | 122.6360 | 23.6264 | 5.455 | $1.39 \times 10^{-8}$ | 143.2690 | 13.5471 | 5.253 | $3.49 \times 10^{-8}$ | (PID, PID) |
| | | (PI, PID) | 122.8690 | 23.6264 | 5.455 | $1.39 \times 10^{-8}$ | 143.1870 | 20.8207 | 3.422 | $9.85 \times 10^{-10}$ | |
| | | (PID, PI) | 119.9310 | 29.2578 | 3.327 | $1.07 \times 10^{-8}$ | 145.8310 | 13.5471 | 5.253 | $3.49 \times 10^{-8}$ | |
| | | (PID, PID) | 120.9570 | 29.2578 | 3.327 | $1.07 \times 10^{-8}$ | 144.6580 | 20.8207 | 3.422 | $9.85 \times 10^{-10}$ | |
| 0.66 | 0.60 | (PI, PI) | 170.1280 | 5.1442 | 4.381 | $4.25 \times 10^{-7}$ | 148.7580 | 13.5471 | 5.253 | $3.49 \times 10^{-8}$ | (PI, PID) |
| | | (PI, PID) | 172.4200 | 5.1442 | 4.381 | $4.25 \times 10^{-7}$ | 147.0120 | 20.8207 | 3.422 | $9.85 \times 10^{-10}$ | |
| | | (PID, PI) | 172.4300 | 13.5167 | 3.475 | $5.67 \times 10^{-10}$ | 147.7720 | 13.5471 | 5.253 | $3.49 \times 10^{-8}$ | |
| | | (PID, PID) | 173.2070 | 13.5167 | 3.475 | $5.67 \times 10^{-10}$ | 147.2870 | 20.8207 | 3.422 | $9.85 \times 10^{-10}$ | |

The mechanism associated with $b_1$ is different. According to Equation (40), the uncertainty directly introduces the residual term $(\hat{b}_1 - b_1)\sqrt{2g\,y_1}$ into the first loop. When $b_1 = 0.54 < \hat{b}_1$, this term is positive: the controller overestimates the actual outlet loss of the first tank. This results in the compensation becoming excessive, which accelerates the rise of the liquid level and explains the increase in overshoot. At the same time, the actual plant discharges less fluid, which reduces the energy required to maintain the level. Therefore, PID remains the best response of the first player, since $119.9310 < 122.6360$ when the second player uses PI and $120.9570 < 122.8690$ when the second player uses PID. The second player also retains PID as their best response, preserving the equilibrium $(\mathrm{PID}, \mathrm{PID})$.

When $b_1 = 0.66 > \hat{b}_1$, the residual term becomes negative: the actual hydraulic loss is larger than that accounted for in the compensation law, and so acts as an additional

disturbance to be rejected. The first player must then provide a larger control effort. With the selected tuning parameters, the auxiliary control inputs take the forms $v_i = 2e_i + \eta_i$ for PI and $v_i = 2e_i + 2\eta_i$ for PID. Therefore, the PID controller exhibits a stronger integral action, which improves the speed of correction but also increases the energy expenditure in the presence of this uncompensated loss. Since the cost function $J_i$ penalizes control energy, PI becomes energetically preferable for the first player: $170.1280 < 172.4300$ against PI and $172.4200 < 173.2070$ against PID. The second player retains PID as their best response, which shifts the equilibrium to $(\mathrm{PI}, \mathrm{PID})$.

The results obtained for uncertainties in $a$ and $b_1$ show that the considered parametric perturbations not only affect transient performance but introduce residual hydraulic terms that modify the level trajectories and control efforts, thereby altering the energy-based ranking of the PI and PID strategies. Since the Nash equilibrium is determined by the best responses associated with the players' costs, a reversal of this ranking may lead to a change in the equilibrium configuration. Nevertheless, the regulation performance remains satisfactory in the considered cases, with convergent liquid levels and small steady-state errors. Hence, the analysis reveals good robustness of the tracking performance together with greater sensitivity to model uncertainties on the part of the strategic controller selection.

## 6. Conclusions

This study formulates loop-wise PI/PID controller structure selection in a coupled two-tank hydraulic system as a finite non-cooperative game. The proposed framework combines exact state-feedback linearization, PI/PID design based on pole placement, and game-theoretic decision-making to account for the interaction between the two regulation loops. Although feedback linearization decouples the auxiliary tracking dynamics, the reconstructed physical pump inputs retain the nonlinear hydraulic coupling. Consequently, the control energy cost of each loop depends not just on its own controller structure but on the structure selected for the neighboring loop. This interdependence justifies treating controller architecture as a strategic design variable rather than as an independent local choice.

For the nominal symmetric configuration, $(\mathrm{PID}, \mathrm{PID})$ is the unique Nash equilibrium, even though $(\mathrm{PI}, \mathrm{PI})$ yields a slightly lower aggregate control energy cost. This result highlights an important distinction between strategic stability and collective energy minimization: a controller assignment may be stable against unilateral deviations without minimizing the total energy expenditure of the interconnected system. The time-domain analysis further shows that PID provides faster settling and a smaller finite-horizon steady-state error at the cost of higher overshoot. The sensitivity analyses demonstrate that controller tuning, leakage, hydraulic coupling, and initial conditions can modify the players' best responses and produce symmetric, asymmetric, or multiple Nash equilibria. The robustness assessment further shows that the considered parametric mismatches can change the energy-based ranking of the PI/PID strategies, and consequently the equilibrium configuration, while convergent level tracking with small steady-state errors is preserved.

Overall, the results show that controller structure selection in an interconnected nonlinear process should explicitly account for the physical coupling and the resulting interaction between local control objectives. The framework in this paper provides a systematic basis for selecting fixed and directly implementable controller architectures at the design stage. The present study is limited to offline selection between PI and PID structures, a control energy-based game criterion, and numerical simulation. In addition, exact feedback linearization relies on sufficiently accurate model information and available liquid level measurements. Future work will focus on dynamic or adaptive controller selection, multi-

criteria formulations combining energy and tracking performance, broader uncertainty and disturbance scenarios, and experimental validation on a physical coupled-tank platform.

**Author Contributions:** Conceptualization, N.N.M.; methodology, N.N.M. and H.L.; software, N.N.M.; validation, N.N.M. and H.L.; formal analysis, N.N.M. and H.L.; investigation, N.N.M.; writing—original draft, N.N.M.; writing—review and editing, N.N.M.; visualization, N.N.M.; supervision, H.L. All authors have read and agreed to the published version of the manuscript.

**Funding:** This research received no external funding.

**Data Availability Statement:** The original contributions presented in this study are included in the article. Further inquiries can be directed to the corresponding author.

**Conflicts of Interest:** The authors declare no conflicts of interest.

## Nomenclature

Main variables, parameters, and symbols used in the manuscript.

| Symbol | Definition | Unit |
|---|---|---|
| $y_i(t)$ | Liquid level in tank $R_i$ | m |
| $y_{i,\mathrm{ref}}$ | Reference liquid level for tank $R_i$ | m |
| $u_i(t)$ | Physical pump inflow applied to tank $R_i$ | $\mathrm{m^3\,s^{-1}}$ |
| $Q_{12}(t)$ | Signed interconnection flow rate between the two tanks | $\mathrm{m^3\,s^{-1}}$ |
| $Q_{i,\mathrm{ext}}(t)$ | External outlet flow rate from tank $R_i$ | $\mathrm{m^3\,s^{-1}}$ |
| $A$ | Cross-sectional area of each tank, $A_1 = A_2 = A$ | $\mathrm{m^2}$ |
| $a$ | Cross-sectional area of the interconnection channel | $\mathrm{m^2}$ |
| $b_i$ | Cross-sectional area of the external outlet of tank $R_i$ | $\mathrm{m^2}$ |
| $g$ | Gravitational acceleration | $\mathrm{m\,s^{-2}}$ |
| $x(t)$ | State vector of the hydraulic system | m |
| $v_i(t)$ | Auxiliary control input after feedback linearization | $\mathrm{m\,s^{-1}}$ |
| $e_i(t)$ | Tracking error, $e_i(t) = y_{i,\mathrm{ref}} - y_i(t)$ | m |
| $K_{P_i}$ | Proportional controller gain | $\mathrm{s^{-1}}$ |
| $K_{I_i}$ | Integral controller gain | $\mathrm{s^{-2}}$ |
| $K_{D_i}$ | Derivative controller gain | – |
| $\lambda$ | Prescribed exponential decay rate of the closed-loop poles | $\mathrm{s^{-1}}$ |
| $\zeta^{\mathrm{PI}}$ | Damping ratio of the PI-controlled dynamics | – |
| $\zeta^{\mathrm{PID}}$ | Damping ratio of the PID-controlled dynamics | – |
| $\mathcal{P}_i$ | Player associated with tank $R_i$ | – |
| $S_i$ | Strategy set of player $\mathcal{P}_i$, $S_i = \{\mathrm{PI}, \mathrm{PID}\}$ | – |
| $s_i$ | Controller structure selected by player $\mathcal{P}_i$ | – |
| $J_i$ | Control-energy-based cost of player $\mathcal{P}_i$ | $\mathrm{m^6\,s^{-1}}$ |
| $T$ | Simulation and cost-evaluation horizon | s |
| $\Delta t$ | Numerical integration time step | s |
| $M_{p,i}$ | Maximum overshoot of tank $R_i$ | % |
| $T_{s,i}$ | Settling time of tank $R_i$ | s |
| $e_{ss,i}$ | Finite-horizon steady-state error | m |

## References

1. Smith, R.S.; Doyle, J. The Two Tank Experiment: A Benchmark Control Problem. In *Proceedings of the 1988 American Control Conference, Atlanta, GA, USA, 15–17 June 1988*; IEEE: Piscataway, NJ, USA, 1988; pp. 2026–2031. [CrossRef]
2. El-Nagar, A.M.; Abdo, M.I. Development of Sliding Mode Control Based on Diagonal Recurrent Neural Network for Coupled Tank System. *Neural Comput. Appl.* **2024**, *36*, 15279–15293. [CrossRef]
3. Teppa-Garrán, P.; Muñoz-de Escalona, D.; Zambrano, J. Liquid Level Tracking for a Coupled Tank System Using Quasi-LPV Control. *Ingenius* **2025**, *33*, 15–26. [CrossRef]
4. Kundu, P.K.; Cohen, I.M.; Dowling, D.R.; Capecelatro, J. *Fluid Mechanics*, 7th ed.; Elsevier: Amsterdam, The Netherlands, 2024.

5. Isidori, A. *Nonlinear Control Systems*, 3rd ed.; Springer: London, UK, 1995.
6. Ackermann, J. Der Entwurf linearer Regelungssysteme im Zustandsraum. *at-Automatisierungstechnik* **1972**, *20*, 297–300. [CrossRef]
7. Roy, P.; Roy, B.K. Fractional Order PI Control Applied to Level Control in Coupled Two Tank MIMO System with Experimental Validation. *Control Eng. Pract.* **2016**, *48*, 119–135. [CrossRef]
8. Roy, P.; Kar, B.; Roy, B.K. Fractional Order PI-PD Control of Liquid Level in Coupled Two Tank System and its Experimental Validation. *Asian J. Control* **2017**, *19*, 1699–1709. [CrossRef]
9. Sorcia-Vázquez, F.d.J.; Rumbo-Morales, J.Y.; Brizuela-Mendoza, J.A.; Ortiz-Torres, G.; Sarmiento-Bustos, E.; Pérez-Vidal, A.F.; Rentería-Vargas, E.M.; De-la-Torre, M.; Osorio-Sánchez, R. Experimental Validation of Fractional PID Controllers Applied to a Two-Tank System. *Mathematics* **2023**, *11*, 2651. [CrossRef]
10. Govind K.R., A.; Mahapatra, S. Frequency Domain Specifications Based Robust Decentralized PI/PID Control Algorithm for Benchmark Variable-Area Coupled Tank Systems. *Sensors* **2022**, *22*, 9165. [CrossRef] [PubMed]
11. Meng, X.; Yu, H.; Zhang, J.; Xu, T.; Wu, H.; Yan, K. Disturbance Observer-Based Feedback Linearization Control for a Quadruple-Tank Liquid Level System. *ISA Trans.* **2022**, *122*, 146–162. [CrossRef] [PubMed]
12. Govind K.R., A.; Mahapatra, S. Improving Precision and Robustness in Level Control of Coupled Tank Systems: A Tree Seed Optimization and $\mu$-Analysis Approach. *Results Control Optim.* **2024**, *15*, 100410. [CrossRef]
13. Ünal, H.U.; Torres-García, D.; Niculescu, S.-I. Robust Least-Fragile PI Controller Design for a Coupled-Tanks System with Uncertain Time-Varying Input Time-Delay. *IFAC-PapersOnLine* **2025**, *59*, 219–224. [CrossRef]
14. Ayten, K.K.; Dumlu, A.; Golcugezli, S.; Tusik, E.; Kalınay, G. Comparative Real-Time Study of Three Enhanced Control Strategies Applied to Dynamic Process Systems. *Appl. Sci.* **2024**, *14*, 9955. [CrossRef]
15. Nursoy, H.; Başçi, A. Comparison of the Performance of Type-1 and Interval Type-2 Fuzzy PI Controllers for Liquid Level Control in a Coupled Tank System. *Erzincan Univ. J. Sci. Technol.* **2024**, *17*, 523–542. [CrossRef]
16. Yesil, B.; Sahin, S. Real-Time Implementation of a Microcontroller-Based Coupled-Tank Water Level Control System with Feedback Linearization and Fuzzy Logic Controller Algorithms. *Sensors* **2025**, *25*, 1279. [CrossRef] [PubMed]
17. Hajji, N.; Maraoui, S.; Bouzrara, K. Robust Distributed Nonlinear Model Predictive Control via Dual Decomposition Approach Based on Game Theory. *J. Frankl. Inst.* **2020**, *357*, 7680–7695. [CrossRef]
18. Umsonst, D.; Sarıtaş, S.; Dán, G.; Sandberg, H. A Bayesian Nash Equilibrium-Based Moving Target Defense Against Stealthy Sensor Attacks. *IEEE Trans. Autom. Control* **2024**, *69*, 1659–1674. [CrossRef]
19. Misra, R.; Wiśniewski, R.; Kallesøe, C.S. Finding Approximate Correlated Equilibrium for Decentralized Control. *IEEE Control Syst. Lett.* **2025**, *9*, 414–419. [CrossRef]
20. Nash, J.F. Equilibrium Points in N-Person Games. *Proc. Natl. Acad. Sci. USA* **1950**, *36*, 48–49. [CrossRef] [PubMed]


**Disclaimer/Publisher's Note:** The statements, opinions and data contained in all publications are solely those of the individual author(s) and contributor(s) and not of MDPI and/or the editor(s). MDPI and/or the editor(s) disclaim responsibility for any injury to people or property resulting from any ideas, methods, instructions or products referred to in the content.